

Central enhancement of nitrogen-to-oxygen abundance ratio in barred galaxies

E. Florido^{1,2}, A. Zurita^{1,2}, I. Pérez^{1,2}, E. Pérez-Montero³, P.R.T. Coelho⁴, and D.A. Gadotti⁵

¹ Dpto. Física y del Cosmos. Campus de Fuentenueva, Universidad de Granada, 18071 Granada, Spain
e-mail:

² Instituto Carlos I de Física Teórica y Computación, Granada, Spain

³ Instituto de Astrofísica de Andalucía, CSIC, Apartado 3004, 18080 Granada, Spain

⁴ Instituto de Astronomia, Geofísica e Ciências Atmosféricas. Universidade de São Paulo, R. do Matão, 1226, 05508-090 São Paulo, SP, Brazil

⁵ European Southern Observatory, Casilla 19001, Santiago 19, Chile

ABSTRACT

Context. Bar-induced gas inflows towards the galaxy centres are recognized as a key agent for the secular evolution of galaxies. One immediate consequence of this inflow is the accumulation of gas in the centre of galaxies where it can form stars and alter the chemical and physical properties.

Aims. Our aim is to study whether the properties of the ionised gas in the central parts of barred galaxies are altered by the presence of a bar, and whether the change in central properties is related to bar and/or parent galaxy properties.

Methods. We use a sample of nearby face-on disc galaxies with available SDSS spectra, morphological decomposition and information on the stellar population of their bulges, to measure the internal Balmer extinction from the $H\alpha$ to $H\beta$ line ratio, star formation rate, and relevant line-ratios to diagnose chemical abundances and gas density.

Results. The distributions of all parameters analysed (internal Balmer extinction at $H\beta$ ($c(H\beta)$), star formation rate per unit area, electron density, $[N II]\lambda 6583/H\alpha$ emission line ratio, ionization parameter and nitrogen-to-oxygen abundance ratio (N/O)) are different for barred and unbarred galaxies, except for the R_{23} metallicity tracer and the oxygen abundance obtained from photoionisation models. The median values of the distributions of these parameters point towards (marginally) larger dust content, star formation rate per unit area, electron density and ionisation parameter in the centres of barred galaxies than in the unbarred counterpart. The most remarkable barred/unbarred difference appears in the $[N II]\lambda 6583/H\alpha$ line ratio, which is on average $\sim 25\%$ larger in barred galaxies, due to a larger N/O in the centres of these galaxies with respect to the unbarred ones. We have analysed these differences as a function of galaxy morphological type (as traced by bulge-to-disc light ratios and bulge mass), total stellar mass and bulge Sérsic index. We observe an enhancement of the differences between central gas properties in barred and unbarred galaxies in later-type galaxies or galaxies with less massive bulges. However the bar seems to have a lower impact on the central gas properties for galaxies with bulges above $\sim 10^{10} M_{\odot}$ or total mass $M_{\star} \geq 10^{10.8} M_{\odot}$.

Conclusions. We find observational evidence that the presence of a galactic bar affects the properties of the ionised gas in the central parts of disc galaxies (radii $\lesssim 0.6$ – 2.1 kpc). The most striking effect is an enhancement in the N/O abundance ratio, which can be qualitatively interpreted, in terms of our current knowledge on bar formation and evolution and on chemical evolution models, as due to a different star formation history in the centres of barred galaxies due to the gas inflow induced by the bar. Our results give support to the scenario in which less and more massive bulges have a different origin or evolutionary process, with the gaseous phase of the former having currently a closer relation with bars.

Key words. Galaxies: evolution – (Galaxies:) bulges – Galaxies: spiral – Galaxies: abundances – Galaxies: ISM – Galaxies: structure – ISM: general

1. Introduction

The distribution of gas and stars in disc galaxies has a basic axisymmetric structure driven by rotation, but superimposed non-axisymmetric morphological features, such as spiral arms or bars are expected to have important consequences on their evolution (e.g. Kormendy & Kennicutt 2004). This *secular*, internally driven, evolution is thought to be dominant in recent times, as opposed to the evolution driven by galaxy hierarchical merging and external gas accretion (e.g. Barnes & Hernquist 1992). Stellar bars have received great attention as important agents for secular galaxy evolution as their non-axisymmetric gravitational potential produces a redistribution of angular momentum of the gas and stars in galactic discs (e.g. Sellwood & Wilkinson 1993; Athanassoula 2003). Gas is dissipative and, at radii well inside

corotation, loses angular momentum as a result of the gravitational torque exerted by the bar and it is therefore driven towards the galaxy centre (e.g. Athanassoula 1992; Friedli & Benz 1993; Friedli et al. 1994). Analytical and numerical simulations also show that the effectiveness to which a bar influences the galaxy dynamics (bar strength) changes as the bar evolves (Athanassoula 2003) and therefore also does the bar-induced gas inflow rate (Regan & Teuben 2004).

According to simulations, bar-induced gas inflow can affect the central properties of galaxies in a number of ways: increase the central gas and dust concentration and trigger star formation (SF) (Friedli & Benz 1993; Martinet & Friedli 1997); produce the formation and growth of a disk pseudobulge (Kormendy & Kennicutt 2004; Cheung et al. 2013) and alter central abundance

and dilute the initial disc metallicity gradient (Friedli & Benz 1993; Friedli et al. 1994). If the gas is able to reach the central parsecs, it could potentially act as fuel for a central massive black hole (Shlosman et al. 1989) and thus form an AGN (e.g. Coelho & Gadotti 2011; Oh et al. 2012). Ultimately, bars can produce central mass concentrations and once they accumulate sufficient mass in the centres they weaken and, for sufficiently high mass, the bar could even get dissolved (e.g. Pfenniger & Norman 1990; Friedli & Benz 1993; Bournaud & Combes 2002), although in more recent simulations bars are more robust than initially thought (e.g. Shen & Sellwood 2004; Athanassoula et al. 2005, 2013). For a detailed description on the role of bars in secular evolution see review by Kormendy & Kennicutt (2004) and references therein.

There is observational evidence for bar-induced gas inflows (e.g. Regan et al. 1997; Zurita et al. 2004). The inflow rate has been measured to range $\sim 0.1\text{--}1\text{ M}_{\odot}\text{ yr}^{-1}$ (Regan et al. 1997; Sakamoto et al. 1999), being higher in earlier-type galaxies (Regan & Teuben 2004; Sheth et al. 2005). However, the observational search for the theoretically predicted effects of bar inflows in the properties of the central gas-phase component of galaxies has not been successful in many cases and conclusions are frequently contradictory.

Barred galaxies have higher central molecular mass concentrations than unbarred galaxies (Sakamoto et al. 1999; Sheth et al. 2005), that produce a higher star formation rate (SFR) in the centres of barred galaxies as observed by a number of authors (e.g. Hummel et al. 1990; Ho et al. 1997b; Wang et al. 2012; Zhou et al. 2015; Ellison et al. 2011; Oh et al. 2012) but there is no agreement on the dependence of this enhancement in SFR with bar properties. For example, Wang et al. (2012) and Zhou et al. (2015) find a positive trend between SFR and ellipticity or ellipticity-based parameters for strong bars, and Oh et al. (2012) with bar length, but no dependency is found by other authors (Pompea & Rieke 1990; Roussel et al. 2001; Ellison et al. 2011). On the other hand, Ellison et al. (2011) find an enhancement in central SFR only for barred galaxies more massive than 10^{10} M_{\odot} and the enhancements observed by Oh et al. (2012) are restricted to the reddest galaxies of their sample. In addition, recently Cacho et al. (2014) find no enhancement in SFR in barred galaxies with respect to unbarred ones.

Studies of the central gas-phase metallicity yielded even more complex results. Ellison et al. (2011) find central oxygen abundances ~ 0.06 dex larger in barred than in unbarred galaxies at a given galaxy stellar mass, but Cacho et al. (2014) find no difference in a similar study to the one performed by Ellison et al. (2011). Other authors (Considère et al. 2000; Dutil & Roy 1999) with a smaller galaxy sample measure lower central oxygen abundances in barred starbursts than in normal unbarred galaxies. No relation has been found so far between bar strength and central oxygen abundance.

Therefore, although simulations predict important effects in the central gas properties of barred galaxies, observationally confirmation has not yet convincingly been found. The same bars that produce an enhancement in SFR do not seem to produce the metallicity alteration that simulations predict (Friedli et al. 1994; Martel et al. 2013). Bar evolution with its accompanying bar strength change, joined to the fact that bars can even be destroyed (so that currently unbarred galaxies maybe had a bar in the past) might be part of the reason for the existing discrepant results. But also, central properties might also depend on the availability of gas and on host galaxy properties in general (namely total mass or Hubble type), which makes sample selection critical.

The advent of the SDSS spectroscopic data has made it possible to study the effects of bars in central gas properties using large galaxy samples and covering wide ranges in host galaxy properties. Although works in this field have contributed with interesting results, all publications so far have focussed on central star-formation, and only in a few cases oxygen abundance has also been studied (Ellison et al. 2011; Cacho et al. 2014). However, bar-induced gas inflows might also alter other physical properties of the central gas. For example, if bars are able to produce larger central mass concentrations (Sakamoto et al. 1999; Sheth et al. 2005), larger concentrations of dust should be expected in the centres of barred galaxies, which would produce larger extinction. This larger concentration of gas and dust in centres of barred galaxies joined to a larger bar-induced SFR could also produce larger electron densities in the centres of barred galaxies (Ho et al. 1997b). The star-formation history in galaxy centres is likely to be different in barred and unbarred galaxies due to the gas supply induced by the bars, which might leave footprints in the nitrogen-to-oxygen (N/O) abundance ratio (Mollá & Gavilán 2010; Mallery et al. 2007; Edmunds & Pagel 1978). It is then worth exploring other properties of the ionised gas which might be modified by the effect of a bar. This is the motivation of the work presented here.

In this paper we will study ionised gas properties in the centres of barred and unbarred galaxies. In addition to the SFR and oxygen abundance, the Balmer extinction, electron density and the N/O abundance ratio will be measured. We will use a sample of nearby galaxies with available spectra from which we will remove AGN. Our galaxy sample has important advantages with respect to previous ones: galaxies are face-on ($i < 26^{\circ}$), the stellar component has already been studied by Coelho & Gadotti (2011) and morphological 2D decomposition, and therefore structural information of bars, bulges and discs, is also available (Gadotti 2009).

Our final aim is to look for observational evidence that bar-induced inflows have important consequences on central properties of the gas, and therefore on secular evolution.

This paper is organized as follows. Sect. 2 describes our galaxy sample. In Sect. 3 we describe the emission line fluxes measurements on which our study is based. Afterwards we remove AGN from the sample (Sect. 4). In Sects. 5, 6, 7 and 8 the internal extinction, central oxygen abundance, nitrogen-to-oxygen ratio, SFR and electron density are calculated for all sample galaxies, and the distribution of these parameters is comparatively analysed for barred and unbarred galaxies separately. In the following sections (9, 10, 11) we explore the dependence of the found differences with the galaxy Hubble type, and with total galaxy and bulge mass, and possible dependencies on bar properties. In Sect. 12 we discuss our results, which are summarized in Sect. 13.

2. Galaxy sample

The galaxy sample used here is the one used by Coelho & Gadotti (2011) to study the stellar populations of the bulges of barred and unbarred galaxies, which is based on the one studied morphologically by Gadotti (2009).

The sample contains all spiral face-on galaxies (axial ratio $b/a \geq 0.9$) in the Sloan Digital Sky Survey (SDSS) Data Release 2, with stellar masses larger than 10^{10} M_{\odot} , redshift $0.02 \leq z \leq 0.07$, bulge-to-total luminosity ratio below 0.043 (i.e. earlier than $\sim \text{Sd}$), and with signal-to-noise ratio in their corresponding SDSS spectra greater or equal than 10, measured over

the spectral range corresponding to the SDSS g -band. This sample comprises 251 barred and 324 unbarred galaxies. The two subsamples of barred and unbarred galaxies have similar total stellar mass distributions (Coelho & Gadotti 2011).

3. Analysis of the spectra

3.1. Spectra pre-processing

The spectra analysed in this paper comes from the SDSS Data Release 7. The spectra pre-processing comprises shifting of the original spectra to the rest frame using the redshifts from the SDSS database, re-sampling in steps of 1\AA , and Galactic extinction correction as described by Cid Fernandes et al. (2005).

Afterwards the emission of the stellar component was modelled with the spectral synthesis code STARLIGHT (Cid Fernandes et al. 2005), by comparing the observed SDSS spectra, in a pixel-by-pixel basis, to stellar population models (Vazdekis et al. 2010).

We refer the reader to Coelho & Gadotti (2011) and Gadotti (2009) and references therein for full details on the sample selection and biases, and on the spectra pre-processing and modelling of the stellar component.

3.2. Emission line measurements

The emission line fluxes have been automatically measured over the stellar emission subtracted SDSS spectra of the galaxy sample, processed as described above.

We have developed a code for measuring the fluxes of the brightest emission lines of the optical spectra. These include $[\text{O II}]\lambda\lambda 3727, 3729$, $\text{H}\delta$, $\text{H}\gamma$, $\text{H}\beta$, $[\text{O III}]\lambda 4959$, $[\text{O III}]\lambda 5007$, $[\text{O I}]\lambda 6300$, $[\text{N II}]\lambda 6548$, $\text{H}\alpha$, $[\text{N II}]\lambda 6584$ and $[\text{S II}]\lambda\lambda 6717, 6731$. All line fluxes were measured independently of each other, with no assumptions on the relative strength of any pair of lines.

In a first step, the code searches for significant emission (over the continuum level) at the rest-frame wavelength of the brightest emission lines. At this point, the continuum level is determined from a linear fit of the median continuum level in two spectral regions at both sides of each emission line. If the code detects an emission peak with signal over the continuum level greater than twice the standard deviation of the continuum, then the emission line profile is fitted with a Gaussian function, and the central wavelength and full-width at half maximum ($fwhm$) of the line are determined. Only fitted emission features yielding reasonable values¹ for the central wavelength and $fwhm$ are considered as true detections. In a second step, the code measures the emission line fluxes. To do this, the code first defines new regions dominated by continuum emission at both sides of each emission line. The size and distance of these *continuum regions* from the emission line central wavelength depend on both the previously determined $fwhm$ and on the location of neighbour emission lines. The continuum level at the emission line position is estimated through a linear fit of the median continuum levels in the *continuum regions*. This is a relevant step in the procedure, as the larger uncertainties in the line fluxes come from the determination of the continuum level. Line fluxes are

then obtained from direct integration of the emission line profiles over the continuum level determined as described above, except for $[\text{N II}]\lambda 6548$, $\text{H}\alpha$, $[\text{N II}]\lambda 6584$ and $[\text{S II}]\lambda\lambda 6717, 6731$, for which fluxes obtained from Gaussian line fitting were adopted in order to ensure accurate flux retrieval in cases in which these sets of lines were blended together.

The preliminary flux measurements were carefully inspected for unreliable measurements and/or undetected emission lines, clearly detectable by eye. These checks have been done interactively, by visual inspection of the individual spectra and on the Gaussian and continuum fits, and with comparisons with measurements done by hand with the SPLAT IRAF² task for random sets of spectra. The code was then modified accordingly until automatic results were in reasonable agreement (within $\sim 20\%$) with by hand flux measurements.

The uncertainty of the line fluxes was estimated by propagating the uncertainty of the continuum level emission in the line flux calculation. Emission line flux measurements with signal-to-noise ratios lower than 3 were rejected and set to zero. Typically, relative errors are below $\sim 5\%$ for line fluxes brighter than $\sim 1.5 \times 10^{-15} \text{ erg s}^{-1} \text{ cm}^{-2}$ for all emission lines, except for $[\text{O II}]\lambda\lambda 3727, 3729$, for which relative errors are larger ($\sim 10\%$) at that flux level. Line flux relative errors increase up to $\sim 20\%$ at flux levels of $\sim 3 \times 10^{-16} \text{ erg s}^{-1} \text{ cm}^{-2}$ for all lines except for $[\text{O II}]\lambda\lambda 3727, 3729$, in which errors are typically larger ($\sim 25\text{--}30\%$).

We have empirically checked the quality of our emission line measurements by comparing the emission line ratios $[\text{N II}]\lambda 6548/[\text{N II}]\lambda 6584$ and $[\text{O III}]\lambda 4959/[\text{O III}]\lambda 5007$ to their theoretical values. This is done in Fig. 1. The emission line fluxes of both doublets correlate well with each other, with correlation coefficients of 0.97 and 0.88 for the $[\text{O III}]$ and $[\text{N II}]$ doublet respectively. The fitted slopes are 0.34 ± 0.01 and 0.37 ± 0.02 for $[\text{O III}]\lambda 4959$ vs. $[\text{O III}]\lambda 5007$ and $[\text{N II}]\lambda 6548$ vs. $[\text{N II}]\lambda 6584$ respectively, which are close to the $\sim 1/3$ theoretical value (Osterbrock & Ferland 2006). The dispersion in the $[\text{N II}]\lambda 6548$ vs. $[\text{N II}]\lambda 6584$ is larger than the one of the $[\text{O III}]$ doublet, specially towards larger values of $[\text{N II}]\lambda 6584/\text{H}\beta$. In general, the galaxies with larger deviation from the best linear fits are also the ones with larger error bars. This fact reinforces our flux error estimates, which seems to represent well real uncertainties in the measurements. Data points with the largest deviation from the best fit are normally AGNs (specially for the $[\text{N II}]$ doublet). We concentrate only on non-AGN galaxies in this paper and therefore our results will not be affected by these larger uncertainties.

3.3. Comparison with emission line fluxes from other databases

We have compared our emission line flux measurements with those available in some public databases. The most popular public databases with emission line fluxes are the MPA-JHU³ release of spectrum measurements (from SDSS DR7) and the OSSY⁴ database (Oh et al. 2011). As in our case, these databases used also the 7th release of the SDSS spectra. MPA-JHU line fluxes of extended sources are normalised to match the photo-

¹ At this stage, we only considered as true detections those features having simultaneously: (a) A maximum central wavelength shift from expected rest-frame wavelength smaller than 4.5\AA , and (b) A $fwhm$ within a factor or two the $fwhm$ of the $[\text{O II}]\lambda\lambda 3727, 3729$ doublet, when the doublet was detected, or a $fwhm$ between 2 and 45\AA when $[\text{O II}]\lambda\lambda 3727, 3729$ was not detected.

² IRAF is distributed by the National Optical Astronomy Observatory, which is operated by the Association of Universities for Research in Astronomy (AURA) under cooperative agreement with the National Science Foundation.

³ <http://www.mpa-garching.mpg.de/SDSS/DR7/>

⁴ <http://gem.yonsei.ac.kr/~kswh/wordpress/>

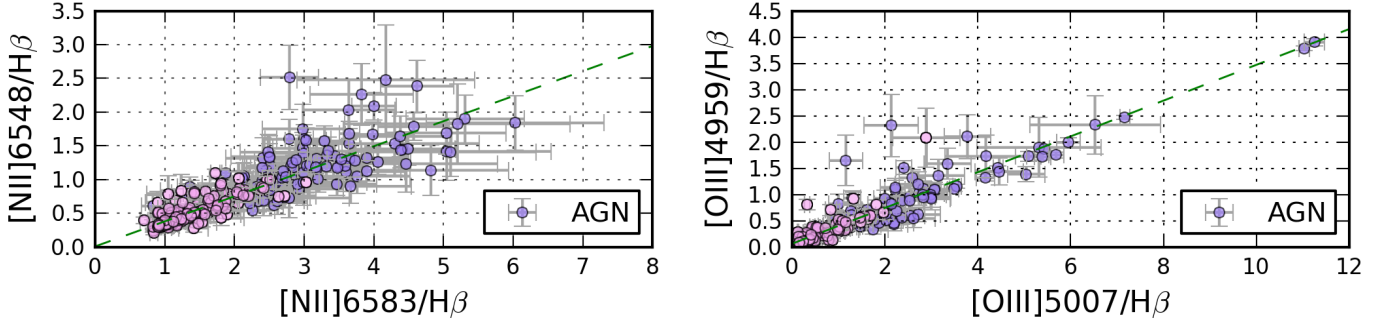


Fig. 1. Comparison of the measured emission line fluxes of the two lines in doublets $[\text{N II}]\lambda\lambda 6548, 6584$ (*left*) and $[\text{O III}]\lambda\lambda 4959, 5007$ (*right*) normalized to the $\text{H}\beta$ emission line flux. Purple points indicate galaxies classified as AGN (Sect. 4). The dashed green line shows the best linear fit to the data, which yields a slope of 0.37 ± 0.02 and 0.34 ± 0.01 for $[\text{N II}]\lambda 6548/\text{H}\beta$ vs. $[\text{N II}]\lambda 6584/\text{H}\beta$ and $[\text{O III}]\lambda 4959/\text{H}\beta$ vs. $[\text{O III}]\lambda 5007/\text{H}\beta$ respectively (see text in Sect. 3.2 for details).

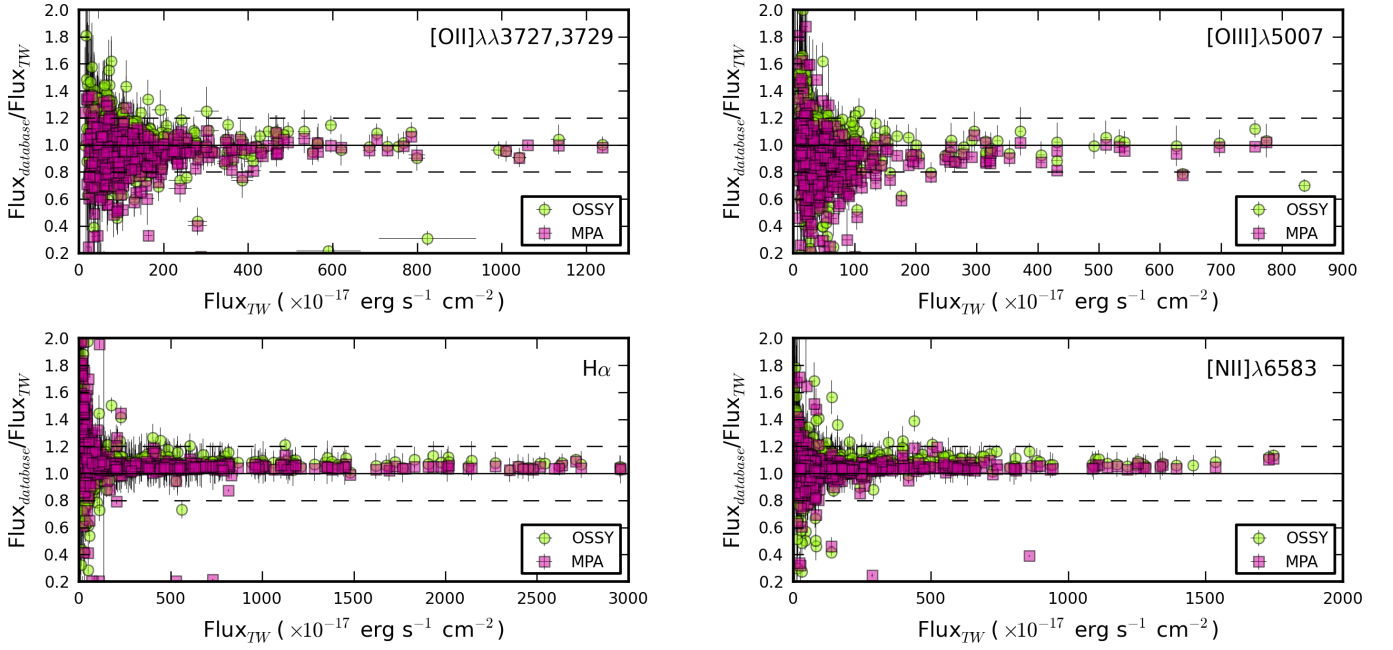


Fig. 2. Ratio of emission line fluxes available in public databases to the fluxes measured in this work (Flux_{TW}), for the OSSY (green circles) and MPA-JHU (pink squares) databases, as a function of the emission line fluxes measured in this work for the $[\text{O II}]\lambda\lambda 3726, 3729$ (top left), $[\text{O III}]\lambda 5007$ (top right), $\text{H}\alpha$ (bottom left) and $[\text{N II}]\lambda 6583$ (bottom right) emission lines. All fluxes are corrected for Galactic extinction (see Sect 3.3 for details).

metric fibre magnitude in the r -band. We have removed this normalization from the MPA-JHU data.

Fig. 2 shows the comparison of the $[\text{O II}]\lambda\lambda 3727, 3729$, $[\text{O III}]\lambda 5007$, $\text{H}\alpha$, and $[\text{N II}]\lambda 6583$ emission line fluxes measured by these databases with our measurements from the spectra of our galaxy sample (Sect. 2). The three sets of data represented in Fig. 2 are corrected for foreground Galactic reddening (not for internal extinction). Our line emission fluxes agree fairly well with those from the OSSY and MPA-JHU databases. In general the fluxes agree within $\sim 20\%$ for lines brighter than $\sim 10^{-15} \text{ erg s}^{-1} \text{ cm}^{-2}$, except for $[\text{O II}]\lambda\lambda 3727, 3729$, in which differences are within $\sim 30\%$. For weaker lines, the scatter increases considerably, due to larger relative errors in the measurements.

For emission lines brighter than $\gtrsim 3 \times 10^{-15} \text{ erg s}^{-1} \text{ cm}^{-2}$, our fluxes agree with the OSSY and MPA-JHU measurements within $\sim 4\text{--}6\%$, except for $[\text{N II}]\lambda 6583$ and $\text{H}\alpha$ as measured by OSSY, which are in average $\sim 8\%$ larger than our measurements. Our measurements of $[\text{N II}]\lambda 6583$ and $\text{H}\alpha$ are also systematically

lower than the ones from MPA-JHU but only by $\sim 4\%$ in average. For $[\text{O II}]\lambda\lambda 3727, 3729$, and $[\text{O III}]\lambda 5007$, however, our measurements are systematically larger than MPA-JHU measurements by $\sim 5\%$, and are in better agreement with the OSSY measurements (within $\sim 2\text{--}3\%$). These systematic differences can in part (but not completely) be due to the usage of different extinction laws for the correction of the foreground Galactic extinction. Our data was corrected using the Schlegel et al. (1998) maps and the Cardelli et al. (1989) extinction curve (see Cid Fernandes et al. 2005). The MPA-JHU data are corrected using O'Donnell (1994). Differences of order $\sim 3\%$ at $[\text{O II}]\lambda\lambda 3727, 3729$ are expected for typical values of $A_V \sim 1 - 1.5$ mag given the differences in the extinction curves. The extinction curve used by OSSY authors is not specified.

In any case, differences between our observed fluxes and the ones available in the OSSY and MPA-JHU databases are small and comparable to measurement errors, even taking into account that the stellar emission subtraction, the flux measurement pro-

cedures, and the foreground Galactic reddening correction differ in the three sets of data.

4. Nuclear classification and removal of AGN

Our initial galaxy sample (see Sec. 2) includes active and *normal* galaxies. We have used standard diagnostic diagrams based on bright emission-line ratios (also known as BPT diagrams, after Baldwin et al. 1981) to separate the galaxies whose dominant mechanism of ionisation is UV radiation from massive young stars (i.e. star-forming galaxies) from those ionised by an active galactic nucleus (AGN). In Fig. 3a and 3b we show the diagnostic diagrams based on our measured (non-extinction corrected⁵) ratios $[\text{O III}]\lambda 5007/\text{H}\beta$ versus $[\text{N II}]\lambda 6584/\text{H}\alpha$, for the barred and unbarred subsamples of galaxies.

The solid line separates star-forming galaxies from AGN according to the predictions of the photoionisation models of Kewley et al. (2001), while the dashed line sets this separation empirically (Kauffmann et al. 2003a). Both lines do not agree, and the number of AGN predicted by Kauffmann et al. (2003a) is larger than the theoretical prediction. We will refer to the galaxies located between the two lines (i.e. classified as star-forming according to Kewley et al. 2001 and as AGN according to Kauffmann et al. 2003a) as *transition objects*. These are also known as *composite* objects and might be a population of objects whose ionisation is in part produced by recent star-formation and in part due to an AGN (Kewley et al. 2006) but they also might include photoionised nuclei with high nitrogen abundance (Pérez-Montero & Contini 2009). For the later reason we will use the Kewley et al. (2001) criteria to remove AGN from our sample. The horizontal dot-dashed line separates the Seyfert region from the Low-Ionisation Nuclear-line Regions area (LINERs; Kewley et al. 2006).

According to this classification into star-forming, transition and AGN galaxies, the percentage of AGN in the subsamples of barred and unbarred galaxies is 31% and 18%, respectively; or equivalently there are ~ 1.7 times more AGN in barred than in unbarred galaxies. This factor keeps when we consider the Kauffmann et al. (2003a) criteria, i.e. AGN (according to Kewley et al. 2001) plus transition objects are 1.7 times more frequent in the subsample of barred galaxies than in the unbarred galaxy subsample⁶. The fraction of AGN in barred galaxies increases when we consider galaxies with low mass bulges. AGN are about 2 times more frequent in barred galaxies than in unbarred galaxies when one considers only bulges less massive than $10^{10.1} M_{\odot}$.

In what follows we will consider all the galaxies of the sample except those classified as AGN. We will refer to them as the *non-AGN galaxies*, and this sample includes star-forming galaxies according to the Kauffmann et al. (2003a) criteria, transition objects, and unclassified galaxies (normally due to the non-detection of relevant emission lines involved in the BPT dia-

Table 1. Number of active and non-active galaxies in the global sample and in the subsamples of barred and unbarred galaxies, according to the BTP diagrams in Figs. 3a and 3b (see Sect. 4 for details).

Type	whole sample	barred subsample	unbarred subsample
Star-forming	139	43	96
Transition	113	66	47
LINER	109	61	48
Seyfert	28	17	11
Unclassified	186	64	122

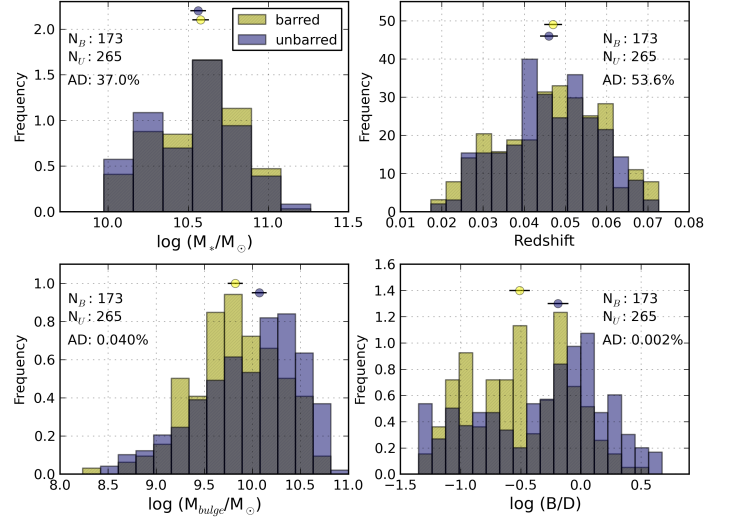


Fig. 4. Histograms showing the distribution of decimal logarithm of the total galaxy stellar mass, redshift, logarithm of bulge mass and logarithm of the bulge to disc light ratio in the *i*-band for barred (hatched yellow) and unbarred (purple) galaxies separately, for all the non-active galaxies of the sample. The number of galaxies in each subsample (N_B and N_U) is indicated, together with the two-sample Anderson-Darling test P -values (AD, expressed in %). The yellow and purple circles in the upper side of the panels indicate the median value of the barred and unbarred distributions respectively. The horizontal error bar covers the 95% confidence interval (estimated as $1.57 \times IQR / \sqrt{N}$, where IQR is the interquartile range, or 1st quartile subtracted from the 3rd quartile, and N the number of data points) for the corresponding median value.

gram). Our effective sample of non-AGN galaxies have 173 and 265 barred and unbarred galaxies, respectively.

4.1. Non-AGN and Star-forming subsamples characterization

Fig. 4 shows a comparison between the total galaxy stellar mass, redshift, bulge mass and bulge-to-disc light ratio (*i*-band) distributions for the subsamples of barred and unbarred galaxies. The total stellar masses are taken from Kauffmann et al. (2003b), and are based on fitting to stellar spectral features (the 4000Å break and the Balmer absorption line index $H\delta_A$). The bulge masses come from Coelho & Gadotti (2011) (based on bulge luminosity and mass-to-light ratio in the *i*-band) and the bulge-to-disc light ratio comes from morphological decomposition performed by Gadotti (2009). The total galaxy stellar mass and redshift distributions are similar for barred and unbarred galaxies. In order to statistically confirm this we have used the k -sample Anderson-Darling (hereinafter A-D) test (see Scholz &

⁵ The $[\text{O III}]\lambda 5007/\text{H}\beta$ versus $[\text{N II}]\lambda 6584/\text{H}\alpha$ is the least reddening dependent BPT plot. After internal extinction correction as described in Sect. 5, we have checked that our classification was correct. BPT diagrams showed in Sect. 12 are based on extinction corrected emission-line fluxes.

⁶ Coelho & Gadotti (2011) used the AGN catalogue from Kauffmann et al. 2003a, <http://www.mpa-garching.mpg.de/SDSS/DR4/Data/agncatalogue.html>, to separate AGN galaxies from the whole sample. Their numbers differ from the ones used in this work, in which classification comes from our emission line measurements. However, in both cases AGN are ~ 1.7 times more frequent in barred than in unbarred galaxies.

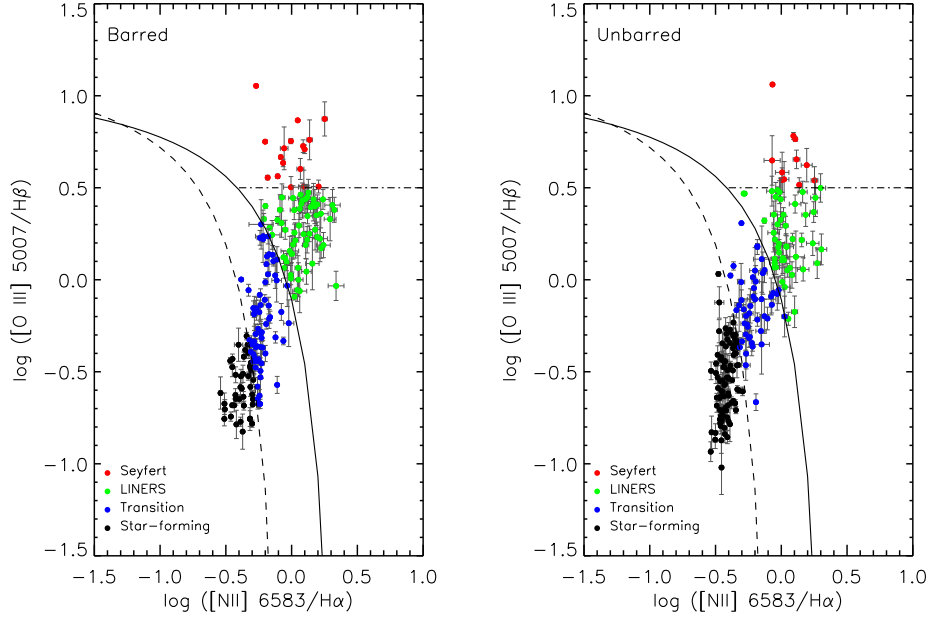


Fig. 3. Diagnostic diagrams to classify emission-line galaxies according to their dominant ionisation mechanism for the barred (*left*) and unbarred (*right*) galaxies of the sample. The solid and dash lines separate the region of star-forming galaxies from the region of AGN according to Kewley et al. (2001) and Kauffmann et al. (2003a), respectively. The horizontal dot-dashed line separates the AGN region into Seyfert and LINER galaxy regions (Kewley et al. 2006).

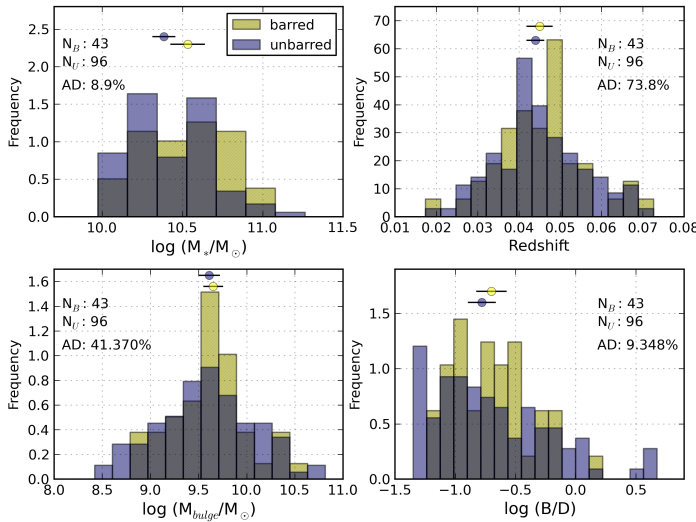


Fig. 5. Same as Fig. 4 but only for galaxies classified as star-forming according to Kauffmann et al. (2003a). N_B and N_U are the number of barred and unbarred galaxies respectively, and AD is the two-sample Anderson-Darling test P -value (expressed in %).

Stephens 1987; Stephens 1974)⁷. The test yields P -values or significance levels at which the null hypothesis that the two samples come from the same parent distribution can not be rejected

⁷ The k -sample Anderson-Darling test is based on the Anderson-Darling rank statistics (Anderson & Darling 1954) for testing homogeneity of samples with possibly different sample sizes and unspecified distributions. The Anderson-Darling test is, in turn, a modification of the Kolmogorov-Smirnov test. The k -sample version of the test is more recommended than k -sample Kolmogorov-Smirnov for small sample sizes (see e.g. Hou et al. 2009). See also discussion at <https://asaip.psu.edu/Articles/beware-the-kolmogorov-smirnov-test>.

of $\sim 37\%$ and 54% for the total stellar mass and redshift respectively. These values are much greater than the 5% threshold value normally adopted, below which the result is statistically significant and the null hypothesis can be rejected. The distributions of bulge mass and bulge-to-disc light ratio are however different between barred and unbarred galaxies when all non-AGN galaxies are considered. Median values and distribution shapes are different, and the A-D tests confirms the difference, with P -values well below 0.1%. The bulges of barred galaxies are less massive than in unbarred galaxies and bulge-to-disc light ratios are also smaller for barred galaxies, even although both subsamples of barred and unbarred galaxies have the same total stellar mass distributions. This was already pointed out by Coelho & Gadotti (2011).

If we consider the subsample containing only galaxies classified as star-forming, Fig. 5 and the A-D test results indicate that the distributions of total stellar mass, redshift, bulge mass and bulge-to-disc light ratio are not different for barred and unbarred galaxies, as P -values are larger than 5% in all cases.

5. Internal extinction

The emission line fluxes were corrected for internal extinction from the Balmer decrement, using the $H\alpha$ to $H\beta$ emission line flux ratio. In the absence of internal dust extinction, the $H\alpha$ to $H\beta$ line flux ratio, $(F_{H\alpha}/F_{H\beta})_{\text{intr}}$ is equal to 2.86, for typical electron temperatures and densities in star forming regions ($T_e \sim 10000$ K and $n_e \sim 100 \text{ cm}^{-3}$), under the case B of the recombination theory (Osterbrock & Ferland 2006). The presence of dust in the interstellar medium increases this line ratio due to differential extinction, and the amount of attenuation can be quantified with the parameter $c(H\beta)$, the internal extinction at the $H\beta$ emission line:

$$(F_{H\beta})_{\text{obs}} = (F_{H\beta})_{\text{intr}} 10^{-c(H\beta)} \quad (1)$$

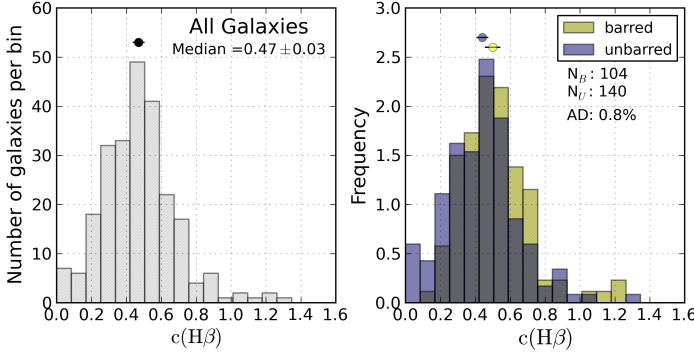


Fig. 6. Left. Histogram of the values of the Balmer extinction at the $H\beta$ emission line, $c(H\beta)$, for all galaxies of the sample with $c(H\beta) > 0.0$ except those classified as AGN as explained in Sect. 4. **Right.** Same as in the left but for barred (hatched yellow) and unbarred (purple) galaxies separately. The number of galaxies in each subsample and the P -value from the A–D test for the two distributions are shown below the figure legend.

where the subindexes ‘obs’ and ‘intr’ stand respectively for observed and intrinsic fluxes. $c(H\beta)$ can be obtained from the $H\alpha$ to $H\beta$ emission line flux ratio, assuming a reddening law⁸ $f(\lambda)$:

$$c(H\beta) = \frac{-1}{f(H\alpha)} \left[\log \left(\frac{F_{H\alpha}}{F_{H\beta}} \right)_{\text{obs}} - \log \left(\frac{F_{H\alpha}}{F_{H\beta}} \right)_{\text{intr}} \right] \quad (2)$$

$f(H\alpha)$ is the reddening function at $H\alpha$ normalized to $H\beta$ (i.e. $f(H\beta) = 0$). We have employed the Seaton (1979) reddening law with the Howarth (1983) parametrisation, assuming $R_V = 3.1$. With this combination of reddening law and R_V , the extinction in magnitudes at $H\alpha$ is $A_{H\alpha} = 1.515 c(H\beta)$. The intrinsic $H\alpha$ to $H\beta$ line flux ratio has been assumed to be 2.86. We are aware that in the central regions of galaxies the metallicity might be oversolar, with T_e lower than 10000 K and therefore this ratio can be larger than 2.9. Assuming a larger value of the $H\alpha$ to $H\beta$ line flux ratio would decrease all $c(H\beta)$ values by 0.02, 0.06 and 0.1 for $(F_{H\alpha}/F_{H\beta})_{\text{intr}}$ equal to 2.9, 3.0 and 3.1 respectively.

The histogram with the values of the Balmer extinction $c(H\beta)$ for all galaxies of the sample (except AGN) is on the left panel of Fig. 6. Values are in the range 0–1.4, being the median value of the distribution (0.47 ± 0.03) . We assign an internal extinction of zero when the observed Balmer ratio $F_{H\alpha}/F_{H\beta}$ is lower than the theoretical value. These objects are not considered in Fig. 6. The obtained distribution is very similar in shape and in values to that found by Stasińska et al. (2004) for 10854 spectra from the First Data Release of the SDSS.

Dust affects both, the stellar continuum emission and the nebular emission. Fig. 7 shows the V -band extinction in magnitudes derived from the gas emission lines ($A_{V,g}$) versus the stellar continuum V -band extinction ($A_{V,s}$) as derived from the spectral synthesis fitting with STARLIGHT (see Sect. 2). We note the reader that the Cardelli et al. (1989) extinction curve was used in STARLIGHT, while we used Seaton (1979) for the gas component. However, both extinction curves gives roughly the same extinction at the V -band (Seaton gives in average a larger extinction by $\sim 0.8\%$ in that spectral range). The dispersion is high, but

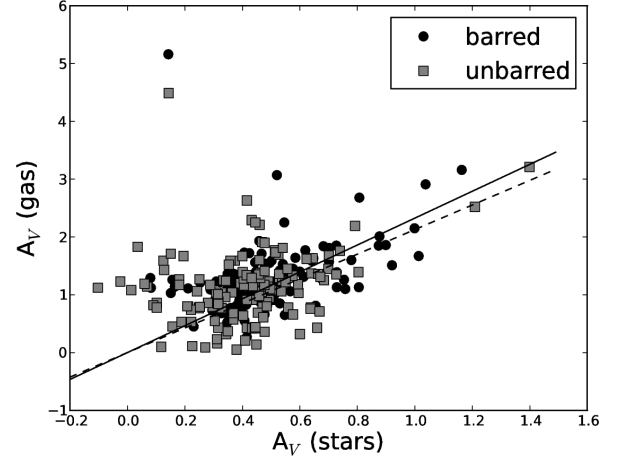


Fig. 7. V -band extinction in magnitudes, $A_{V,g}$, as obtained from the $H\alpha$ to $H\beta$ Balmer decrement, versus the stellar continuum V -band extinction ($A_{V,s}$) as derived from the spectral synthesis fitting with STARLIGHT for all non-AGN galaxies. The straight solid and dashed lines show the relations between $A_{V,g}$ and $A_{V,s}$ found by Calzetti et al. (2000) and Kreckel et al. (2013), respectively.

it is clear from the figure that both quantities are correlated, and that the extinction derived from emission lines is typically about twice the extinction derived from the observed stellar continuum. This is in agreement with other author results, as e.g. Calzetti et al. (2000) and Kreckel et al. (2013), who find $A_{V,g} = (0.44 \pm 0.03) A_{V,s}$ and $A_{V,s} = (0.470 \pm 0.006) A_{V,g}$, respectively, for H II regions and starburst galaxies. These relations are overplotted in Fig. 7 and are compatible with our data in the range of extinction observed ($A_{V,g}$ from 0 to 3 mag).

All measured emission lines were corrected for internal dust extinction using the derived values for $c(H\beta)$. The corrected emission line fluxes have been compared with the corresponding values provided in one of the most popular public databases: OSSY (Oh et al. 2011). Fig. 8 shows comparison of extinction corrected fluxes for some of the brightest emission lines. As it can be seen, OSSY fluxes are typically larger than our extinction corrected line fluxes by a factor of about 1.6 (~ 1.8 for [O II]). Also, the OSSY colour excess tabulated values for the gas and the stellar continuum (called $E(B-V)_{\text{gas}}$ and $E(B-V)_{\text{star}}$, respectively) do not hold the relation mentioned above (Fig. 7).

However, we remark here that our observed (uncorrected) emission line fluxes are in good agreement with their quoted observed fluxes (see Sect. 3.3 and Fig. 2).

A table containing extinction corrected line fluxes measured in this paper are available at the CDS. The table contains the following information: Column 1 gives the SDSS plate used to collect the spectrum, Column 2 the modified Julian Date of the observation night (mjd), Column 3 the SDSS fiber number, Columns 4 to 25 the extinction corrected emission line fluxes normalised to $H\beta = 100$ and associated uncertainties, Columns 25 and 27 give the $H\beta$ flux in units of $10^{-17} \text{ erg s}^{-1} \text{ cm}^{-2}$ and the Balmer extinction at $H\beta$, respectively, and Columns 26 and 28 their corresponding uncertainties.

5.1. $c(H\beta)$ distribution for barred and unbarred galaxies

The right panel of Fig. 6 shows the distribution of $c(H\beta)$ for barred and unbarred galaxies separately. The median value of $c(H\beta)$ is only marginally larger in barred (0.50 ± 0.04) than in unbarred galaxies (0.44 ± 0.03), but the A–D test indicates that

⁸ The relation of $f(\lambda)$ with the function $X(x)$ of the Howarth (1983) parametrisation is $f(\lambda) = \frac{X(x)}{X(x_{H\beta})} - 1$, where $x = 1/\lambda$ (λ in microns) with $x_{H\beta}$, the corresponding value for the $H\beta$ spectral line. In this parametrisation, the extinction in magnitudes at a given wavelength λ is $A_\lambda = X(x) E(B - V)$.

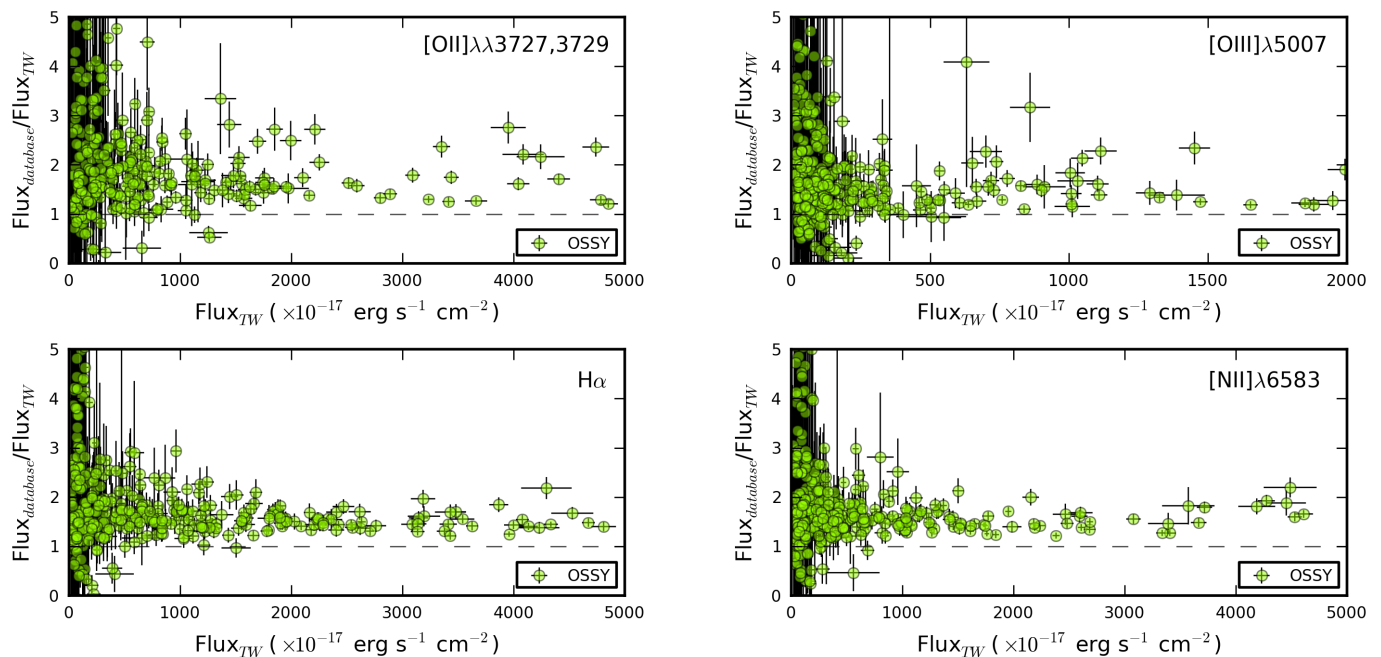


Fig. 8. Ratio of internal extinction corrected emission line fluxes from the OSSY database to the ones measured in this work, as a function of the later for the [O II]λλ3726,3729 (top left), [O III]λ5007 (top right), Hα (bottom left) and [N II]λ6583 (bottom right) emission lines. All fluxes have been corrected of Galactic extinction and internal extinction (see Sect. 5 for details).

the two distributions are different, with a P-value of 0.8%, well below 5%. We find the same result when we only consider star-forming galaxies (see Table 2).

Previous work on the Balmer extinction at Hβ on large SDSS data samples (e.g. Stasińska et al. 2004) has shown that $c(\text{H}\beta)$ decreases from early to late-type galaxies. $c(\text{H}\beta)$ also depends on total galaxy luminosity, being larger for the most luminous galaxies (and likely more massive). Our subsample of barred non-AGN galaxies is similar to the unbarred subsample in terms of total stellar mass (Fig. 4), but it is biased towards lower bulge mass and lower bulge-to-disc light ratios with respect to the subsample of unbarred galaxies. If we assume that Stasińska et al. (2004) results for integrated spectral properties of galaxies, is applicable to the inner kiloparsec of galaxies, we would predict a lower average $c(\text{H}\beta)$ in barred than in unbarred galaxies, just the opposite of what we find, although differences in median values are only marginal (within error bars).

The subsamples of barred and unbarred star-forming galaxies (Fig. 5) are equivalent in bulge-to-disc light ratios, and bulge mass and their distributions of $c(\text{H}\beta)$ are also different (P-value 0.6%), being larger in barred than in unbarred galaxies by ~ 0.07 dex, approximately the same difference than between the non-AGN barred/unbarred subsamples. A larger central dust extinction might be related with a larger dust mass surface density (Kreckel et al. 2013) and therefore, the observed difference in $c(\text{H}\beta)$, although marginal, could be due to different central dust mass concentrations possibly due to the transfer of material towards the galaxy centres induced by bars.

6. Central oxygen abundance and N/O abundance ratio

The faint auroral emission lines are not generally detected in our optical spectra and then the electron temperature (T_e) can not be calculated. Therefore, it is not possible to determine abundances

from the T_e -based or *direct* method and the oxygen abundance can only be inferred through empirical or theoretical calibrations of nebular strong-line flux ratios, the *strong-line methods* (see e.g. Pérez-Montero & Díaz 2005; López-Sánchez et al. 2012, for in-depth discussions on different methods). We have used two of the most widely used tracers of gas oxygen abundance: $R_{23} \equiv ([\text{O III}]\lambda\lambda 4959, 5007 + [\text{O II}]\lambda\lambda 3727)/\text{H}\beta$, and $\text{N2} \equiv \log([\text{N II}]\lambda 6583/\text{H}\alpha)$. R_{23} was first proposed by Pagel et al. (1979), but there are many different empirical and theoretical calibrations of this parameter (e.g. Pilyugin 2001; Pilyugin & Thuan 2005; McGaugh 1991; Kewley & Dopita 2002; Kobulnicky & Kewley 2004). The N2 was first proposed by Storch-Bergmann et al. (1994) and it has been extensively used, specially for intermediate and high redshift studies, as the lines involved are readily accessible observationally with the current generation of telescopes, and the line ratio is insensitive to reddening corrections due to the small wavelength separation between the two involved lines. Some of the most common calibrations of N2 include Denicoló et al. (2002), Pettini & Pagel (2004), Nagao et al. (2006) or Pérez-Montero & Contini (2009).

Our aim is to investigate potential differences between barred and unbarred galaxies, and therefore for the moment we will only compare strong-line oxygen abundance indicators, without applying any of the existing calibrations. Fig. 9 shows the comparison of the distribution of values for the R_{23} and N2 parameters for barred and unbarred non-AGN galaxies. Barred and unbarred galaxies seem to be indistinguishable in terms of the median value and distribution of the R_{23} parameter. There is however a striking difference in N2: barred galaxies have enhanced $\log([\text{N II}]\lambda 6583/\text{H}\alpha)$, with respect to unbarred galaxies by 0.10 dex (see Table 2) with both distributions significantly different according to the A-D test (P-value below 0.001%). The two distributions of N2 are also different when considering only star-forming galaxies (P-value 0.002%), having also larger N2 in barred than in unbarred galaxies, but the difference in me-

Table 2. Median values and errors (95% confidence interval of the median) of the distributions of $c(\text{H}\beta)$, R_{23} and N2 gas metallicity indicators, star formation rate per unit area, $[\text{S II}]\lambda 6717/[\text{S II}]\lambda 6731$ line ratio, oxygen abundance and nitrogen-to-oxygen ratio, and logarithm of the ionisation parameter, in the centres of barred and unbarred galaxies in the subsamples of non-AGN and pure star-forming galaxies (Sect. 4) and number of galaxies in each subsample. The P -values of the k -sample Anderson-Darling test for the comparison of distributions for barred and unbarred galaxies are shown for all cases.

	P -value ^a	Non-AGN				P -value ^a	Star-Forming			
		barred median	N	unbarred median	N		barred median	N	unbarred median	N
$c(\text{H}\beta)$	0.8%	0.50 ± 0.04	104	0.44 ± 0.03	140	0.6%	0.53 ± 0.04	43	0.46 ± 0.04	96
$\log R_{23}$	64.0%	0.31 ± 0.04	105	0.31 ± 0.04	130	0.3%	0.19 ± 0.04	41	0.22 ± 0.04	86
N2	0.0009%	-0.28 ± 0.02	110	-0.38 ± 0.02	152	0.02%	-0.37 ± 0.03	43	-0.43 ± 0.01	96
$\log \Sigma_{\text{SFR}}$	0.07%	-1.1 ± 0.1	112	-1.3 ± 0.1	155	0.1%	-0.9 ± 0.1	43	-1.2 ± 0.1	96
$[\text{S II}]\lambda 6717/[\text{S II}]\lambda 6731$	0.05%	1.25 ± 0.03	104	1.31 ± 0.03	127	0.7%	1.28 ± 0.03	40	1.33 ± 0.03	84
$\log (\text{N/O})$	0.01%	-0.49 ± 0.03	105	-0.58 ± 0.03	143	0.03%	-0.49 ± 0.04	40	-0.58 ± 0.03	91
$12 + \log (\text{O/H})$	4.3%	8.68 ± 0.01	107	8.69 ± 0.01	151	7.4%	8.69 ± 0.01	40	8.70 ± 0.01	92
$\log U$	5.3%	-3.08 ± 0.02	107	-3.14 ± 0.02	151	2.5%	-3.09 ± 0.03	40	-3.18 ± 0.02	92

Notes.

^(a) P -value for the Anderson-Darling test, or approximate significance level at which the null hypothesis that the two samples are drawn from the same population can be rejected. Usually, significance levels lower than 5% are requested to reject the null hypothesis.

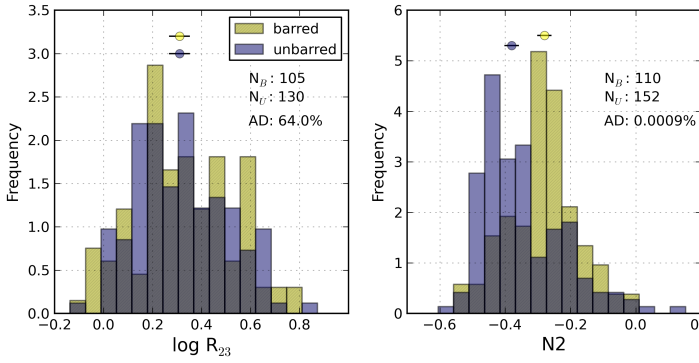


Fig. 9. Histograms of the values of the oxygen abundance indicators $R_{23} = ([\text{O III}] + [\text{O II}])/\text{H}\beta$ (left) and $\text{N2} = \log([\text{N II}]\lambda 6583/\text{H}\alpha)$ (right) for all non-AGN barred and unbarred galaxies of the sample. The number of objects in each subsample and the P -values from the A-D test are shown in each panel.

dian values shortens to ~ 0.06 dex, which is in any case much larger than the uncertainties in the median values.

It is well known that there is a positive mass-metallicity relation for spirals (e.g. Tremonti et al. 2004; Bothwell et al. 2013). We will analyse in detail the dependence of N2 and R_{23} with total stellar mass in Sect. 10. However, we remind the reader here that the mass distributions of our barred and unbarred subsamples are identical and therefore the observed difference in N2 might be indicating a real and strong physical difference in the centres of barred galaxies with respect to unbarred galaxies.

Given that there are no differences between barred and unbarred galaxies in terms of the R_{23} parameter, any empirical calibration of this parameter yields no difference in oxygen abundance between barred and unbarred galaxies. The opposite happens with calibrations which make use of N2 , except for the N2 empirical calibration by Pérez-Montero & Contini (2009), which includes a correction to account for the nitrogen-to-oxygen ratio. We have estimated $\log (\text{N/O})$ from the empirical calibration of the N2S2 ratio ($= \log([\text{N II}]\lambda 6583/[\text{S II}]\lambda 6717, 6731)$) from the same authors. Afterwards, $12 + \log(\text{O/H})$ is calculated. We have also estimated $\log (\text{N/O})$, $12 + \log(\text{O/H})$ and the ionisation pa-

rameter⁹, U , from the new grids of photoionisation models by Pérez-Montero (2014). The results are shown in Table 2 and in Fig. 10. The barred and unbarred subsamples of galaxies have the same average oxygen abundance within errors, $12 + \log(\text{O/H}) = 8.69 \pm 0.01$, and the distributions are indistinguishable from each other: we obtain A-D P -values of 4.3% and 7.4% when we consider non-AGN or star-forming galaxies, respectively. This is in agreement with recent results from Cacho et al. (2014) for a similar sample of barred and unbarred nearby disc galaxies from the Nair & Abraham (2010) catalogue. However, our result is in apparent disagreement with Ellison et al. (2011), who reported a larger oxygen abundance (by ~ 0.06 dex) in barred with respect to unbarred galaxies, for a galaxy sample also extracted from Nair & Abraham (2010). In Sect. 12 we will discuss these results and try to explain the possible sources of discrepancy between their and our results.

However, as expected from the N2 values, we find a statistically significant and interesting difference in the central nitrogen-to-oxygen abundance ratio between barred and unbarred galaxies. The median $\log (\text{N/O})$ is 0.09 dex larger in barred than in unbarred galaxies, for both the non-AGN and the star-forming samples. This difference is three times larger than the uncertainties in the median values (~ 0.03 dex). The AD-test confirms that the barred and unbarred distributions are different (mid-panel in Fig. 10), with P -values of 0.01% and 0.03% for the non-AGN and the star-forming samples, respectively. To our knowledge, this is the most evident and larger difference in physical properties of the gas observed so far between barred and unbarred galaxies.

⁹ Regarding the ionisation parameter values derived from the grid of photoionisation models from Pérez-Montero (2014), it is important to stress that in absence of emission line ratios sensitive to the electron temperature, an empirical law between $\log U$ and $12 + \log(\text{O/H})$ is assumed (i.e. lower U for higher O/H). Nevertheless, in the grid a certain range of variation in $\log U$ is allowed for each O/H value that exceeds the expected and reported $\log U$ variations in our sample of studied objects, so we think that the resulting $\log U$ values give an accurate idea of the variations.

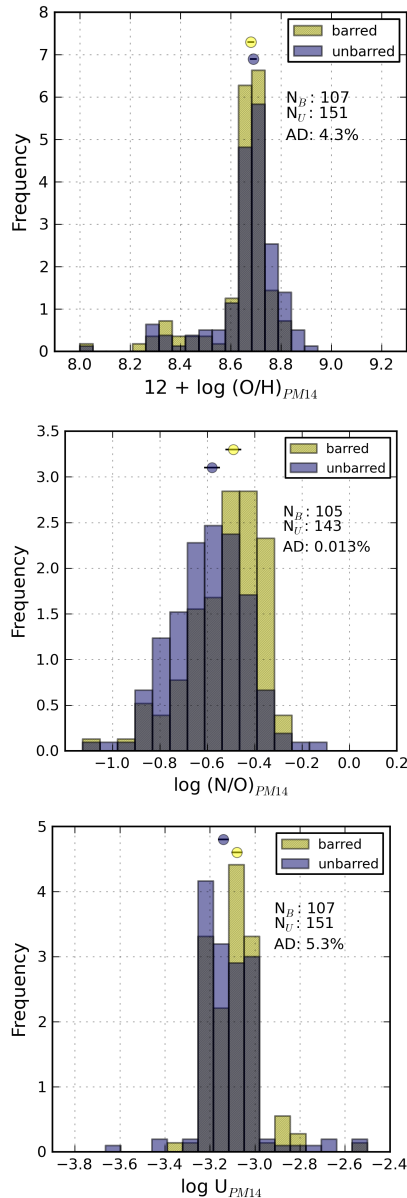


Fig. 10. Histograms of the oxygen abundance (*top*), nitrogen-to-oxygen ratio (*middle*) and ionisation parameter (*U*, *bottom*), as calculated with the Pérez-Montero (2014) method for all non-AGN barred and unbarred galaxies of the sample. The number of objects in each subsample and the P -values from the A-D test are shown below the legend. Only non-AGN galaxies are considered.

7. Star formation rate

We have estimated the star formation rate (SFR) in the galaxy centres from the $\text{H}\alpha$ extinction-corrected emission within the $3''$ SDSS fibres and the Kennicutt (1998) conversion factor¹⁰. The distances to the galaxies have been estimated from the redshift given by SDSS and a Hubble constant of $72 \text{ km s}^{-1} \text{ Mpc}^{-1}$.

Given the redshift range of the galaxy sample, the SDSS $3''$ diameter fibre corresponds to a projected size ranging from ~ 1.2 to 4.2 kpc . Although the redshift range is small and the redshift distributions of barred and unbarred galaxies are similar, we have

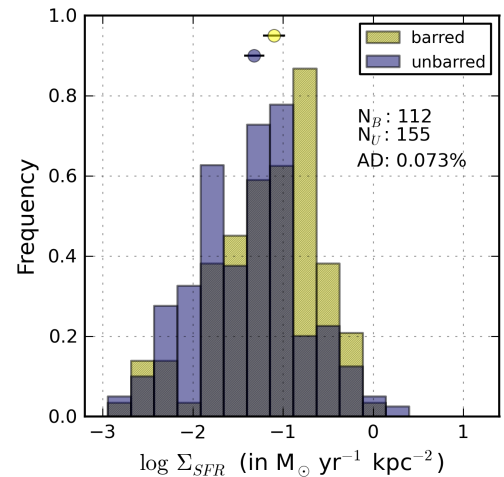


Fig. 11. Comparative histograms of star formation rate per unit area for all non-AGN barred (yellow hatched) and unbarred (purple) galaxies of the sample.

derived star formation rates per unit area, Σ_{SFR} , in order to average out possible dependences on galaxy distance.

The distributions of the logarithm Σ_{SFR} for barred and unbarred galaxies are shown in Fig. 11. Both distributions are different according to the A-D test (P -value $< 0.1\%$) and barred galaxies show marginally larger star formation rate per unit area. This difference is slightly larger when considering only star-forming galaxies, where barred galaxies show a median $\log \Sigma_{\text{SFR}}$ which is ~ 0.3 dex larger than unbarred galaxies.

A larger SFR in the centres of barred galaxies was also reported by Ellison et al. (2011) for the galaxies of similar total stellar mass from a similar study and by other authors (see e.g. Hummel et al. 1990; Ho et al. 1997b; Wang et al. 2012; Oh et al. 2012; Zhou et al. 2015).

8. Electron density

The $[\text{S II}]\lambda 6717/[\text{S II}]\lambda 6731$ line ratio is sensitive to the electron density (N_e). Nearly 8% of all galaxies in our sample have a $[\text{S II}]\lambda 6717/[\text{S II}]\lambda 6731$ line ratio which is above the low-density theoretical limit ($=1.43$, implying $N_e \sim 1 \text{ cm}^{-3}$, for $T_e=10000\text{K}$ Shaw & Dufour 1994). Most of these targets have the largest $[\text{S II}]\lambda 6717/[\text{S II}]\lambda 6731$ relative errors ($\sim 20\text{--}40\%$). We are here considering only galaxies in which their $[\text{S II}]\lambda 6717/[\text{S II}]\lambda 6731$ line ratio value is still compatible with being below the low-density theoretical limit taking into account their corresponding error bars (López-Hernández et al. 2013). The median value of this line ratio in the centres of the non-AGN galaxy sample is 1.29 ± 0.02 (1.30 ± 0.02 for pure SF galaxies), which corresponds to $N_e \sim 100 - 150 \text{ cm}^{-3}$. This is in agreement with typical values in centres of galaxies measured previously by Kennicutt et al. (1989) and Ho et al. (1997a). In Fig. 12 we compare the distributions $[\text{S II}]\lambda 6717/[\text{S II}]\lambda 6731$ for barred and unbarred non-AGN galaxies. The median value is marginally lower for barred (1.25 ± 0.03) than for unbarred galaxies (1.31 ± 0.03), indicating that on average, barred galaxies tend to possess a larger central electron density than unbarred galaxies. The A-D test yields a very low P -value (0.05%), indicating that both distributions are different. Distributions are also different in the subsample of pure star-forming galaxies (P -value of 0.7%, see Table 2).

¹⁰ The stellar component had already been subtracted from the original SDSS spectra and therefore we do not have to correct for stellar absorption under the Balmer lines at this point.

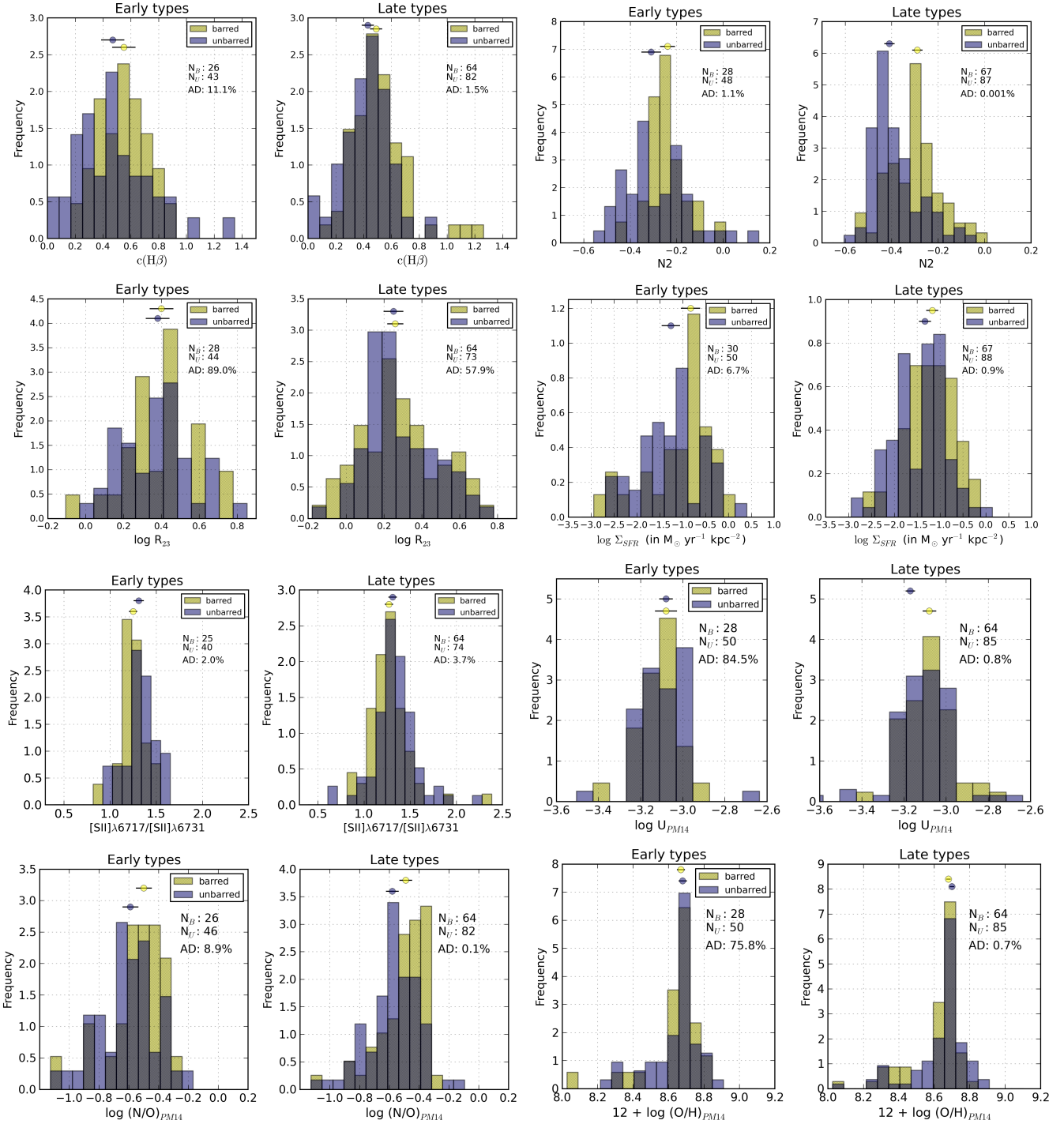


Fig. 13. Comparative histograms of (from top to bottom and from left to right): the Balmer extinction at the $H\beta$ emission line, $c(H\beta)$, N2, $\log R_{23}$, decimal logarithm of the SFR per unit area, $[SII]\lambda 6717/[SII]\lambda 6731$ line ratio, logarithm of the ionisation parameter, nitrogen-to-oxygen abundance ratio and oxygen abundance for barred (yellow, hatched) and unbarred (purple) galaxies separately for early- and late-type galaxies. The separation between early- and late-type galaxies has been done using the bulge to disc luminosity ratio as described in Sect. 9 for the non-AGN subsample of galaxies.

9. Dependence of barred/unbarred central differences with galaxy Hubble type

The amount of gas bar driven towards galaxy centres might depend among others on the availability of gas in galaxy discs and on the gravitational torque created by the bar-like mass distribution. The gas content varies across the Hubble sequence, but also bars in early-type galaxies tend to be longer and stronger

than in late-type spirals (Erwin 2005; Chapelon et al. 1999). Our subsamples of non-AGN galaxies are not similar in terms of bulge-to-disc flux ratio and bulge mass (Fig. 4), which might indicate that both subsamples are different in the relative population of morphological types. We next explore whether any of the differences between barred and unbarred galaxies found in previous sections could be due to a bias towards earlier types in the subsample of barred galaxies.

Table 3. Median values and errors (95% confidence interval of the median) of the distributions of $c(\text{H}\beta)$, R_{23} and N2 gas metallicity indicators, star formation rate per unit area, $[\text{S II}]\lambda 6717/[\text{S II}]\lambda 6731$ line ratio, logarithm of the ionisation parameter, nitrogen-to-oxygen abundance ratio and oxygen abundance in the centres of barred and unbarred galaxies in the subsamples of early and late-type galaxies as defined in Sect. 9 and number of galaxies in each subsample. Only non-AGN galaxies are considered. The P -values of the k -sample Anderson-Darling test for the comparison of distributions for barred and unbarred galaxies is shown for all cases.

	Early-type (based on B/D)					Late-type (based on B/D)				
	P -value	barred median	N	unbarred median	N	P -value	barred median	N	unbarred median	N
$c(\text{H}\beta)$	11.1%	0.55 ± 0.08	26	0.47 ± 0.08	43	1.5%	0.49 ± 0.04	64	0.43 ± 0.04	82
$\log R_{23}$	89.0%	0.40 ± 0.06	28	0.38 ± 0.06	44	57.9%	0.26 ± 0.04	64	0.25 ± 0.05	73
N2	1.1%	-0.24 ± 0.03	28	-0.31 ± 0.04	48	0.001%	-0.29 ± 0.03	67	-0.41 ± 0.01	87
$\log \Sigma_{\text{SFR}}$	6.7%	-0.8 ± 0.2	30	-1.3 ± 0.2	50	0.92%	-1.17 ± 0.12	67	-1.33 ± 0.12	88
$[\text{S II}]\lambda 6717/[\text{S II}]\lambda 6731$	2.0%	1.25 ± 0.04	25	1.31 ± 0.05	40	3.7%	1.27 ± 0.04	64	1.31 ± 0.04	74
$\log U$	85%	-3.08 ± 0.05	28	-3.08 ± 0.03	50	0.8%	-3.08 ± 0.03	64	-3.17 ± 0.02	85
$\log (\text{N/O})$	8.9%	-0.50 ± 0.05	26	-0.59 ± 0.05	46	0.05%	-0.49 ± 0.04	64	-0.58 ± 0.04	82
$12+\log (\text{O/H})$	76%	8.67 ± 0.02	28	8.68 ± 0.02	50	0.7%	8.68 ± 0.01	64	8.70 ± 0.01	85

Table 4. Same as Tables 2 and 3 but for the subsamples of low and high stellar mass bulges.

	$M_{\text{bulge}} < 10^{9.7} M_{\odot}$					$M_{\text{bulge}} \geq 10^{9.7} M_{\odot}$				
	P -value	barred median	N	unbarred median	N	P -value	barred median	N	unbarred median	N
$c(\text{H}\beta)$	0.2%	0.46 ± 0.03	50	0.42 ± 0.04	68	58%	0.52 ± 0.07	54	0.50 ± 0.06	72
$\log R_{23}$	49%	0.31 ± 0.05	49	0.25 ± 0.05	56	67%	0.34 ± 0.06	56	0.35 ± 0.05	74
N2	0.001%	-0.30 ± 0.03	54	-0.43 ± 0.02	68	3.0%	-0.26 ± 0.03	56	-0.33 ± 0.04	84
$\log \Sigma_{\text{SFR}}$	0.45%	-1.15 ± 0.13	54	-1.37 ± 0.12	68	2.6%	-0.99 ± 0.17	58	-1.29 ± 0.16	87
$[\text{S II}]\lambda 6717/[\text{S II}]\lambda 6731$	0.97%	1.26 ± 0.03	53	1.34 ± 0.05	57	2.0%	1.25 ± 0.05	51	1.31 ± 0.03	70
$\log U$	2.9%	-3.08 ± 0.03	51	-3.18 ± 0.02	65	54%	-3.07 ± 0.03	56	-3.09 ± 0.03	86
$\log (\text{N/O})$	0.3%	-0.51 ± 0.04	52	-0.63 ± 0.04	63	0.3%	-0.47 ± 0.04	53	-0.56 ± 0.03	80
$12+\log (\text{O/H})$	0.9%	8.69 ± 0.01	51	8.70 ± 0.02	65	43%	8.67 ± 0.02	56	8.67 ± 0.01	86

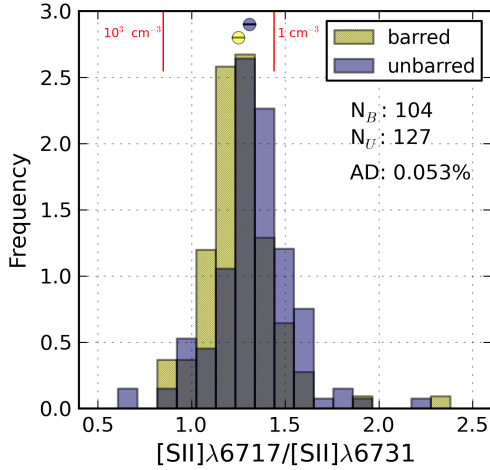


Fig. 12. Comparative histograms of values of the $[\text{S II}]\lambda 6717/[\text{S II}]\lambda 6731$ line ratio for barred (yellow hatched) and unbarred (purple) galaxies separately. Only non-AGN galaxies are considered.

The fact that most of the differences between barred and unbarred galaxies of the non-AGN subsample are also observed in the pure star-forming subsample, where the distribution of bulge mass and bulge-to-disc flux ratio (hereinafter B/D) are equivalent for barred and unbarred galaxies (Fig. 5), seems to indicate that, even if a bias were present, bars tend to produce higher dust concentrations, larger N/O ratios, star formation and electron densities in the centre of galaxies. A deeper analysis is

in any case necessary in order to disentangle the nature of these differences.

Morphological classification is only available for ~46% of the total galaxy sample, i.e. 245 galaxies of which 113 are barred and 132 unbarred. This classification comes from the Nair & Abraham (2010) catalogue. However, morphological decomposition of the galaxy sample has already been performed using the code BUDDA v2.1¹¹ (de Souza et al. 2004; Gadotti 2008, 2009) which is able to fit up to four different galactic components (a bulge with a Sèrsic profile, a single or double exponential disc, a Sèrsic bar and a Moffat central component) to a galaxy image. The morphological decomposition of the galaxies of this sample was performed over SDSS g , r and i -band images (Gadotti 2009) and the B/D flux ratios for the three photometric bands were therefore obtained.

The behaviour of the B/D flux ratio along the Hubble sequence is well known. However, this relation has a high dispersion and strongly varies depending on the function used to fit the bulge ($R^{1/4}$ vs. Sèrsic $R^{1/n}$), on the photometric band or on the galaxy inclination and dust-extinction (see Graham & Worley 2008, and references therein). We have analysed the dependence of the logarithm of the g , r and i -band B/D light ratios obtained with BUDDA (Gadotti 2009) with the T-type by Nair & Abraham (2010) for the galaxies in common between both samples. From these relations and additional information from the Galaxy-Zoo2 catalogue (Willett et al. 2013), we have separated all galaxies in our sample into early (T-type < 2) and late-types

¹¹ <http://www.sc.eso.org/~dgadotti/budda.html>

($T\text{-type} \geq 2$). For more information on this separation we refer the reader to Appendix A.

The bulge stellar light and therefore its mass, has been claimed as a key parameter that might distinguish galaxies across the Hubble sequence (see e.g. Meisels & Ostriker 1984; Graham & Worley 2008, and references therein). In addition to the B/D light ratios we have also used the bulge mass (Coelho & Gadotti 2011) to explore whether the observed differences between barred and unbarred galaxies are dependent on Hubble types. We have separated all non-AGN galaxies into two groups attending to their bulge mass. The dividing bulge mass ($10^{9.7} M_{\odot}$) has been selected to ensure that the total stellar galaxy mass distributions for barred and unbarred galaxies are equivalent in both bulge mass bins (with AD P -values greater than 10%).

Fig. 13 and Table 3 show a comparison of central properties between barred and unbarred galaxies separately for early- and late-type disc galaxies (using B/D light ratios as explained above). The same comparison is made in Fig. 14 and Table 4 for galaxies with bulge mass below than $10^{9.7} M_{\odot}$ and bulge masses larger or equal than $10^{9.7} M_{\odot}$. It can be seen that for galaxies with later types (or less massive bulges) the distributions of all parameters except $\log R_{23}$ are different between barred and unbarred galaxies, with AD P -values lower than 4% in all cases. For earlier type galaxies results depend on whether we split galaxies attending to B/D light ratios or bulge mass. Barred and unbarred earlier type galaxies (according to B/D) only show different distributions for $N2$ and the $[S II]\lambda 6717/[S II]\lambda 6731$ emission-line ratio, while for galaxies with bulge mass above $10^{9.7} M_{\odot}$, in addition to those parameters, we also find different distributions for Σ_{SFR} and $\log (N/O)$.

Barred galaxies tend to have on average larger central Balmer $H\beta$ extinction, larger values of the $N2$ metallicity indicator, SFR per unit area, electron densities and N/O abundance ratio than unbarred galaxies in all subsamples. However, taking into account the uncertainties in the median values, we can not claim real differences in average values between those parameters in barred and unbarred galaxies, apart from the $N2$ parameter and the N/O abundance ratio. $N2$ is clearly larger in barred late-type (by ~ 0.12 dex) and lower bulge-mass (by ~ 0.13 dex) galaxies with respect to unbarred galaxies, while this difference is smaller (~ 0.07 dex) but still significant in the early-type and higher bulge mass subsample. These barred/unbarred differences in $N2$ translate in a larger N/O abundance ratio in barred galaxies by ~ 0.12 dex in low bulge-mass galaxies, and ~ 0.09 dex, in early-type, late-type and higher bulge-mass subsamples.

Finally, if we restrict our comparative analysis of barred/unbarred galaxies to pure star-forming galaxies, we find the same result as with the non-AGN galaxies: late-type galaxies differ in central properties depending on whether they have or not a bar, with barred galaxies exhibiting larger Σ_{SFR} , $c(H\beta)$, $N2$, $\log (N/O)$ and $\log U$, and lower $[S II]\lambda 6717/[S II]\lambda 6731$ than unbarred galaxies. Also, similarly to the non-AGN sample, the distribution of $12 + \log (O/H)$ is different between barred and unbarred late type galaxies and those with smaller bulge mass, with a marginally larger oxygen abundance in unbarred with respect to barred galaxies. The results for late-type galaxies in both the pure star-forming and non-AGN samples, only differ for $\log R_{23}$ which shows a different distribution for barred and unbarred galaxies in the SF sample (although with identical median values). However, in the non-AGN sample the distributions are identical in barred/unbarred galaxies (P -value 58%). The number statistics are poorer for SF galaxies, but it shows

that the inclusion of the *transition objects* is not dominating our main results. We will further comment about this in Sect. 12.

In summary, we observe statistically significant differences in distributions of parameters for barred and unbarred galaxies in our later-type galaxy subsample regardless of whether we select them according to their predicted T -type (from their B/D light ratio) or their bulge mass. These appear in all parameters except in the metallicity tracer R_{23} .

Median values are only marginally different in most parameters (except in $N2$ and $\log (N/O)$), but they point towards a larger Σ_{SFR} , $c(H\beta)$, $N2$, $\log (N/O)$ and $\log U$, and lower $[S II]\lambda 6717/[S II]\lambda 6731$ in barred galaxies. Results for earlier-type galaxies depend on whether we select them attending to B/D light ratio or bulge mass, but with both splitting criteria the distributions of $N2$ and $[S II]\lambda 6717/[S II]\lambda 6731$ are significantly different between barred and unbarred galaxies. The difference in the median value of $N2$ for barred and unbarred galaxies is slightly smaller than in later-type galaxies but still significant.

10. Barred/unbarred difference trends with total galaxy and bulge mass

Previous authors found observational evidence that massive barred galaxies have a higher current central star formation rate than unbarred galaxies of the same stellar mass (Ellison et al. 2011). On the other hand, we have seen above that the effect of bars in the galaxy centres seems to be stronger or more visible in galaxies with lower bulge mass even when the barred and unbarred subsamples have been created to have indistinguishable total stellar mass distributions.

In order to better inspect our own and previous author results, we have created a series of boxplots showing the variation of all parameters as a function of bulge and total stellar mass. Boxplots are an useful representation in our case, as sample sizes are not big enough to explore parameter dependences using histograms. Fig. 16 shows boxplots for $c(H\beta)$, $N2$, $\log R_{23}$, Σ_{SFR} , $[S II]\lambda 6717/[S II]\lambda 6731$, $\log U$, N/O and oxygen abundance as a function of total galaxy stellar mass. See caption of this figure for a description on basic boxplots features. It is clear from these plots that for the most massive galaxies there is only significant difference between barred and unbarred galaxies for the N/O abundance ratio. The most massive galaxies are also the galaxies with more massive bulges, and this result simply confirms the results from Sect. 9. For less massive galaxies ($M_{\star} \lesssim 10^{10.8} M_{\odot}$), $N2$ and Σ_{SFR} are clearly higher for barred than for unbarred galaxies with non-overlapping box-notches between barred and unbarred galaxies in the two lowest mass intervals. Our results are therefore only partially in agreement with Ellison et al. (2011). We do find a larger fibre SFR in barred galaxies above $10^{10} M_{\odot}$, but we do not see differences in SFR between barred and unbarred galaxies above $\sim 10^{10.8} M_{\odot}$.

The differences between barred and unbarred galaxies are undoubtedly better correlated with bulge stellar mass (see Fig. 17). All properties (except R_{23} , $\log U$ and $12 + \log (O/H)$) are significantly different between barred and unbarred galaxies for bulge masses $\lesssim 10^{10.0} M_{\odot}$, but differences normally increase towards lower bulge masses, except for $c(H\beta)$ in the lowest mass bin, in which the median values are similar within errors for both types of galaxies. The observed differences go always in the sense that barred galaxies present larger dust extinction, star formation rate per unit area, $[N II]/H\alpha$ line ratio, lower $[S II]\lambda 6717/[S II]\lambda 6731$ (indicating a higher electron density) and larger $\log (N/O)$ and $\log U$ in their centres.

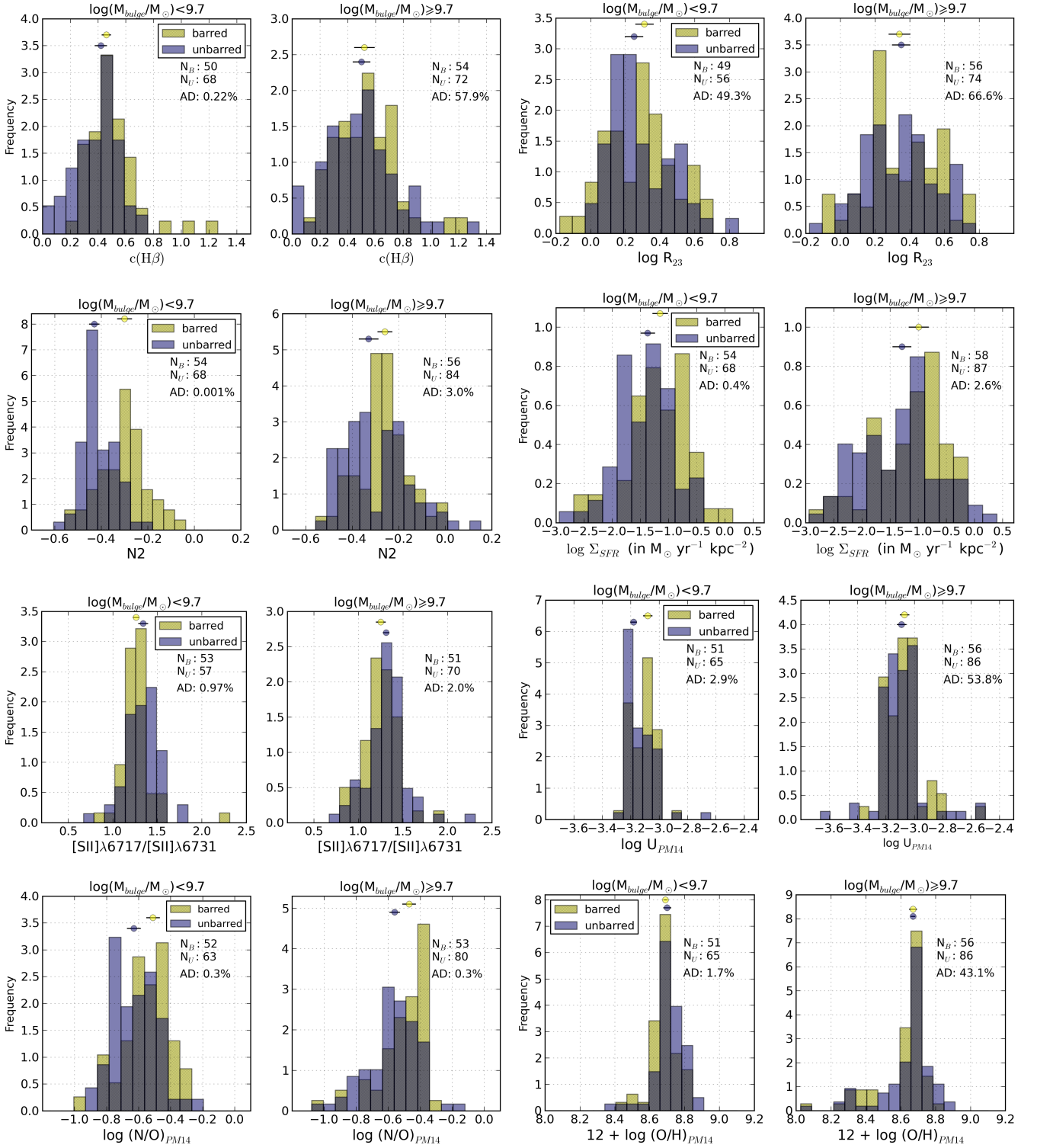


Fig. 14. Comparative histograms of (from top to bottom and from left to right): the Balmer extinction at the $\text{H}\beta$ emission line, $c(\text{H}\beta)$, R_{23} , N_2 , logarithm of the ionisation parameter, logarithm of the SFR per unit area, the $[\text{SII}]\lambda 6717/[\text{SII}]\lambda 6731$ line ratio, logarithm of the ionisation parameter, nitrogen-to-oxygen abundance ratio, and oxygen abundance for barred (yellow, hatched) and unbarred (purple) galaxies separately for non-AGN galaxies with bulge mass lower than $10^{9.7} M_{\odot}$ and for galaxies with heavier bulges ($\geq 10^{9.7} M_{\odot}$).

We note also that the SFR per unit area is also larger in average for barred galaxies in the highest bulge mass bin. However, as mentioned above, we do not see differences in Σ_{SFR} between barred and unbarred galaxies in the most massive galaxies (Fig. 16). This is probably due to the fact that bulge masses of barred galaxies are lower than in unbarred galaxies for the

most massive galaxies (Fig. 15), as already pointed by Coelho & Gadotti (2011).

More massive bulges are typically classical bulges, with Sèrsic indexes higher than ~ 2.5 , in contrast with the so called *pseudo-bulges*, whose surface brightness profile is better fitted with lower Sèrsic indexes and which are typically less massive

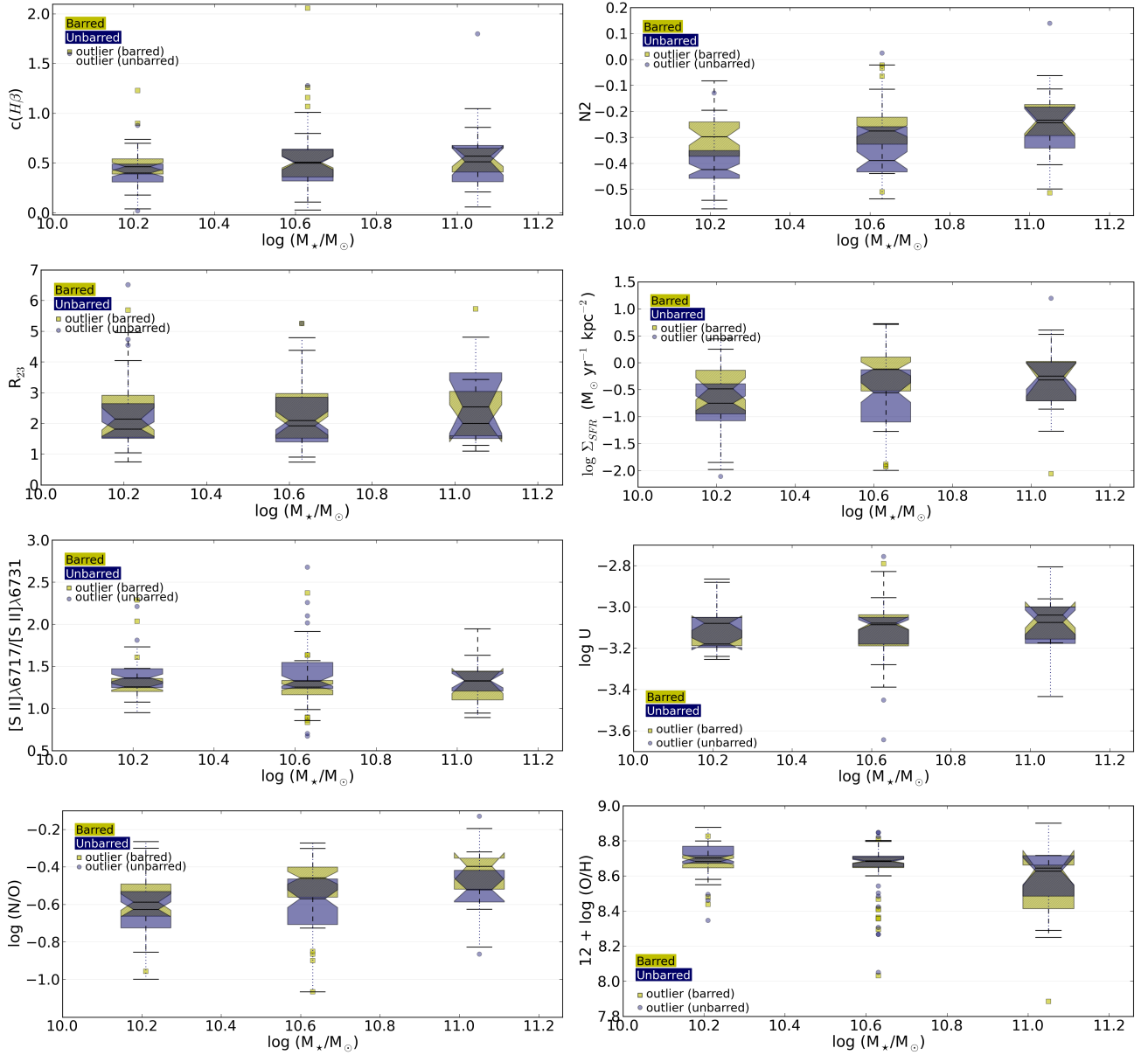


Fig. 16. Boxplots showing the distribution in $c(\text{H}\beta)$, $\text{N2} = \log([\text{N II}]\lambda 6583/\text{H}\alpha)$, R23 , SFR per unit area and $[\text{S II}]\lambda 6717/[\text{S II}]\lambda 6731$ line ratio, decimal logarithm of the ionisation parameter, nitrogen-to-oxygen abundance ratio and oxygen abundance, as a function of the total galaxy stellar mass (M_*) for barred (yellow boxes) and unbarred (purple) galaxies. Each box represent the data distribution for galaxies in a 0.42 dex interval of logarithm in stellar mass centred at the abscissa axis values of the box position. Inside each box, the central horizontal black straight line marks the median value. The lower and upper quartiles are represented by the outer edges of the boxes; i.e. the box length is equal to the inter-quartile range, and therefore the box encloses 50% of the data points. The notches mark the 95% confidence interval for the median value. The whiskers extend to the most extreme data point within 1.5 times the inter-quartile range. Galaxies that do not fall within the reach of the whiskers are considered as outliers (yellow and purple circles for barred and unbarred galaxies respectively). The number of galaxies in each box, in order of increasing stellar mass, ranges from 35 to 39, 55 to 59 and 13 to 14 for barred galaxies, and from 57 to 64, 58 to 70, and 15 to 21, for unbarred galaxies.

than classical bulges (Gadotti 2009). We have also analysed the barred/unbarred galaxy central properties as a function of Sèrsic index. Barred and unbarred galaxies with large values of the Sèrsic index ($n \geq 3.1$) do not differ in their central ionised gas properties, apart from the SFR, which seems to be enhanced in barred galaxies, in agreement with the result found for barred galaxies with the most massive bulges. However the global parameter dependences with the Sèrsic index and the differences between barred and unbarred galaxies are not as clear as with bulge mass or even total stellar mass.

11. Dependence on bar parameters

Previous sections show clear differences in the central ionised gas properties between barred and unbarred galaxies. These differences imply that the gas flows induced by bars are able to modify gas properties, specially in lower mass or lower bulge mass galaxies. Simulations predict a dependence of the gas inflow rate with bar strength, with stronger bars supplying gas towards the centre at a higher rate (Athanasoula 1992; Regan & Teuben 2004). It is then natural to wonder whether these observational enhancements are related to dynamical or structural bar parameters.

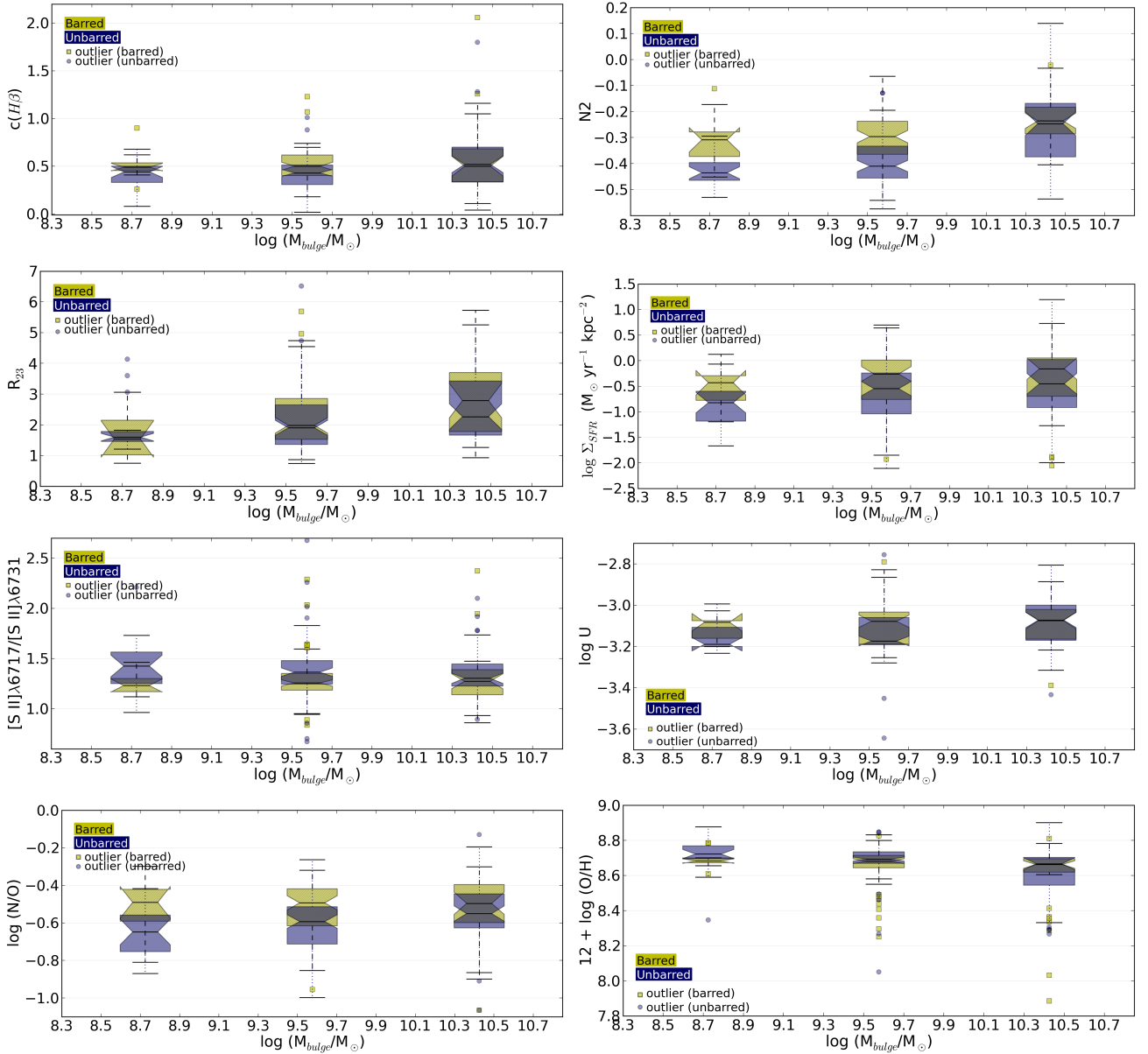


Fig. 17. Same as Fig. 16 but as a function of the bulge mass. Each box represents the data distribution for galaxies in a 0.85 dex interval of logarithm in bulge stellar mass centred at the abscissas values of the box position. The number of galaxies in each box, in order of increasing stellar bulge mass, ranges from 9 to 10, 66 to 71 and 28 to 32 for barred galaxies, and from 18 to 22, 70 to 81, and 28 to 32, for unbarred galaxies.

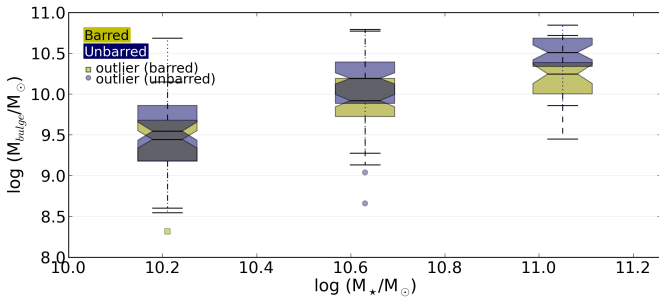


Fig. 15. Boxplot showing median values of bulge stellar mass for three different bins in total galaxy stellar mass.

Morphological decomposition of the galaxy sample was performed by Gadotti (2009) and a number of structural parameters for discs, bulges and bars (in the case of barred galaxies) are then

available. This allows for a comparison between parameters such as bar ellipticity (as a proxy for bar strength) and bar strength with central ionised gas properties. Our results are presented and compared with previous work in the next paragraphs.

We find weak trends for the SFR per unit area (Σ_{SFR}) to increase with the bar effective radius, the bar semi-major axis normalised to the galaxy disc scale length or the bar ellipticity, but the dispersion is high and the Spearman rank correlation coefficients (ρ_s) are 0.28, 0.20 and 0.12 respectively. For other parameters, such as the bar Sérsic index (which might be related to the bar age; Kim et al. 2014) ρ_s is lower than 0.1. This is in agreement with previous works on central SFRs from infrared emission (e.g. Pompea & Rieke 1990; Roussel et al. 2001), who did not find evidence that stronger bars could produce a larger enhancement in SFRs. Ellison et al. (2011) in turn, did not find correlation between bar length and fibre SFR in the central region of galaxies from SDSS optical spectra. However, other au-

thors did report a positive relation between central star formation and bar parameters, but their results are in some cases conflicting: Oh et al. (2012) report a higher effect of bars on central SF but only for the reddest galaxies and the effects are more pronounced with increasing bar length. On the other hand, other authors (Wang et al. 2012) find that only strong bars can enhance central SF, but the degree of enhancement depends only on bar ellipticity, and not on bar size or bar mass, in agreement with Zhou et al. (2015), who find a weak positive trend between SFR in bulges and an ellipticity-based bar strength parameter.

Several studies have also tried to confirm observationally the effect of bars on the central oxygen abundance and on the radial oxygen abundance gradient (see e.g. Florido et al. 2012, and references therein), but results are also conflicting. For example, there is disagreement on whether bars produce a larger oxygen abundance in galaxy centres (e.g. Ellison et al. 2011), equal than in unbarred galaxies (e.g. Chapelon et al. 1999; Cacho et al. 2014) or whether O/H is lower in barred galaxies than in galaxies without a stellar bar (Considère et al. 2000; Dutil & Roy 1999). However there seems to be a consensus that neither central nor the O/H abundance gradient depend on bar strength (Chapelon et al. 1999; Considère et al. 2000; Cacho et al. 2014; Ellison et al. 2011). Our results agree with previous work, as we also find no clear trend between $12+\log(\text{O}/\text{H})$ and bar parameters (effective radius, normalised length, ellipticity) with correlation coefficients ρ_S lower than 0.2, with a slightly better correlation with the bar boxiness ($\rho_S=0.32$).

We also find no correlation between the N/O abundance ratio and any bar parameter, with ρ_S lower than 0.1 in all cases, with the exception of a weak trend for the N/O to increase with the bar effective radius ($\rho_S=0.15$). $c(\text{H}\beta)$ and the $[\text{N II}]\lambda 6717/[\text{N II}]\lambda 6731$ emission line ratio do not show any clear dependence on bar parameters either ($\rho_S \lesssim 0.2$).

12. Discussion

In this paper we comparatively analyse the properties of the ionised gas in the centres of disc galaxies that possess a stellar bar, with those without a bar structure. Our analysis is based on SDSS spectra.

The SDSS fibre size ($3''$) and our face-on galaxy sample redshift range ($0.02 \leq z \leq 0.07$) implies that in this work we are analysing emission of the ionised gas located within galactocentric radii between approximately 0.6 and 2.1 kpc. The ionised gas emitting regions located at these galactocentric distances are usually termed as *nuclear H II regions* or *H II region nucleus* when they are located in the immediate neighbourhood of a galactic centre, and *hotspots* or *circumnuclear H II regions* when these regions surround the galaxy centre, frequently arranged in a ring or pseudo-ring shape (see e.g. Kennicutt et al. 1989; Ho et al. 1997a; Díaz et al. 2007). The spectroscopic studies of nuclear and circumnuclear spatially resolved H II regions are still limited to a small number of targets. These have focussed the attention of previous in depth spectroscopic studies but mainly with the aim of comparing its physical and stellar content properties with those of normal disc H II regions (see e.g. Kennicutt et al. 1989; Ho et al. 1997a; Bresolin & Kennicutt 2002), studying differences in properties with host galaxy Hubble type (Ho et al. 1997a) and/or deriving chemical abundances for these regions, expected to be the ones with highest metal content due to its location in the inner parts of spiral discs (Díaz et al. 2007; Dors et al. 2011). To our knowledge there is no published work so far comparing the properties of resolved nuclear and circum-

nuclear H II regions in barred and unbarred galaxies for a large number of galaxies and in a systematic way.

Our derived values for internal Balmer extinction, $[\text{N II}]\lambda 6717/[\text{N II}]\lambda 6731$ ratio, oxygen abundance and N/O ratio are within the values quoted by authors analysing individual, resolved nuclear and circumnuclear H II regions (e.g. Kennicutt et al. 1989; Bresolin & Kennicutt 2002; Díaz et al. 2007; Dors et al. 2008).

Our result that the current star formation rate and electron density (as traced by $[\text{N II}]\lambda 6717/[\text{N II}]\lambda 6731$) are also larger in barred systems is also in agreement with Ho et al. (1997b), who made a spectroscopic survey of the nuclei (using a $2'' \times 4''$ aperture) of nearly 500 nearby galaxies. In particular, they found a larger star formation rate only in barred galaxies earlier than Sbc with respect to the unbarred counterparts, with no difference between barred and unbarred late-type spirals. We also find a larger average SFR per unit area in barred galaxies in our early-type subsample (see Fig. 13) but the distributions for barred and unbarred galaxies are only marginally different, while the difference in both distributions is statistically different for the late-type galaxies, according to the AD test. We should remind the reader that the most significant differences between barred and unbarred galaxies (in all gas properties) are obtained for lower bulge/total stellar mass galaxies (i.e. later-type galaxies). The total stellar galaxy or bulge mass distribution for Ho et al. (1997b) galaxy sample is not shown and we can not further compare both results.

12.1. Enhanced $[\text{N II}]\lambda 6583/\text{H}\alpha$ in centres of barred galaxies

The most striking difference between barred and unbarred galaxies obtained in this work comes from the observed $[\text{N II}]\lambda 6583/\text{H}\alpha$ emission line ratio.

An enhanced $[\text{N II}]\lambda 6583/\text{H}\alpha$ emission line ratio in the galaxy centres was first found by Stauffer (1982) and later by different authors (see e.g. Kennicutt et al. 1989; Ho et al. 1997a; Sanchez et al. 2014). Ho et al. (1997a) analysed the integrated spectra of a sample of 206 galaxy nuclei. They reported that early-type galaxies had the largest $[\text{N II}]\lambda 6583/\text{H}\alpha$. According to these authors, it might be an indication that nitrogen is selectively enriched in the centres of bulge-dominated galaxies. This is in agreement with the general trend found in this work (without distinction between barred and unbarred systems), as early-type galaxies are also in average more massive and host more massive bulges than late-type galaxies (see Figs. 16 and 17). In this work we go a step forward and show that this line ratio is larger in the centres of barred galaxies and that the bar effect in enhancing this line ratio is more important in galaxies with less massive bulges.

A number of effects can enhance the $[\text{N II}]\lambda 6583$ to $\text{H}\alpha$ emission line ratio, namely the nitrogen excitation by a different source to photoionisation (i.e. AGN or shocks), which enhances the $[\text{N II}]$ emission with respect to emission from recombination lines, and a larger abundance of nitrogen atoms with respect to oxygen.

We will now analyse these cases separately. We have used the criteria by Kewley et al. (2001) based on the $[\text{O III}]\lambda 5007/\text{H}\beta$ vs. $[\text{N II}]\lambda 6583/\text{H}\alpha$ to remove AGN from the galaxy sample. This separation criteria allows for objects of the *composite* area to be included, which may add a number of galaxies in which shocks or an AGN can enhance the $[\text{N II}]\lambda 6583$ emission, but also pure photoionised objects with high N/O ratio (Pérez-Montero & Contini 2009). We remind the reader that pure SF galaxies also show a significant difference in $[\text{N II}]\lambda 6583/\text{H}\alpha$ between barred

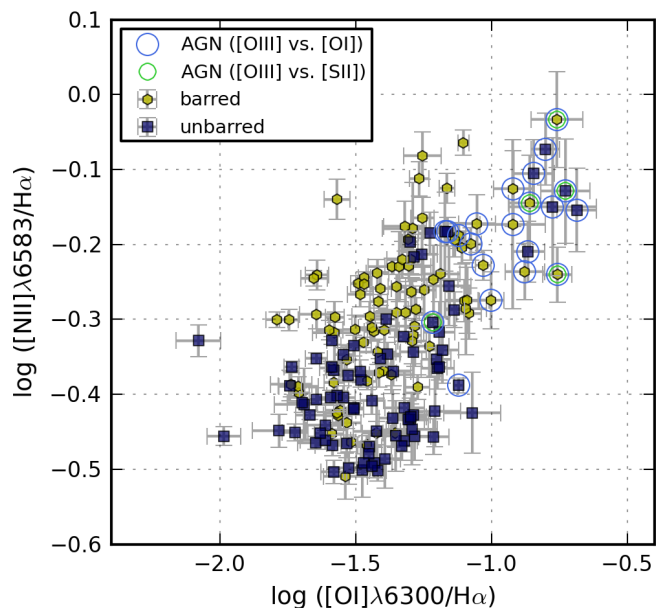


Fig. 18. Comparison of shock and AGN sensitive emission line ratios $[\text{N II}]\lambda 6583/\text{H}\alpha$ and $[\text{O I}]\lambda 6300/\text{H}\alpha$ for barred and unbarred galaxies. Galaxies that would be considered as AGN according to the $[\text{O III}]/\text{H}\beta$ vs. $[\text{O I}]/\text{H}\alpha$ or $[\text{O III}]/\text{H}\beta$ vs. $[\text{S II}]/\text{H}\alpha$ diagrams and the Kewley et al. (2006) separation line are marked with blue and green circles respectively.

and unbarred galaxies (see Table 2). However, in order to check whether the use of Kewley et al. (2001) criteria is including a high number of shock ionised barred galaxies, and therefore enhancing the observed differences (e.g. in the right panel of Fig. 9) between barred and unbarred galaxies, we have created Fig. 18. The figure shows $[\text{N II}]\lambda 6583/\text{H}\alpha$ as a function of the shock and AGN sensitive $[\text{O I}]\lambda 6300/\text{H}\alpha$ line ratio. We can see that the galaxies with large $\log([\text{O I}]\lambda 6300/\text{H}\alpha)$ in their centres ($\gtrsim -1$) are also galaxies with high $[\text{N II}]\lambda 6583/\text{H}\alpha$ and, according to the $[\text{O III}]\lambda 5007/\text{H}\beta$ vs. $[\text{O I}]\lambda 6300/\text{H}\alpha$ BPT diagram, those galaxies would have been classified as AGN (Kewley et al. 2006, encircled in blue). However there is roughly the same number of barred (11) and unbarred (10) galaxies in that area of the plot. Of those galaxies, only 3 barred galaxies and 2 unbarred galaxies would have been classified as AGN also with the $[\text{O III}]\lambda 5007/\text{H}\beta$ vs. $[\text{S II}]\lambda 6717,6731/\text{H}\alpha$ diagram and the separation line given by Kewley et al. (2006), encircled in green. The plot clearly shows that even removing those galaxies, the average $[\text{N II}]\lambda 6583/\text{H}\alpha$ is larger in barred than in unbarred galaxies.

In addition, if shocks or AGN excitation were responsible for a larger $[\text{N II}]\lambda 6583/\text{H}\alpha$ in barred galaxies, we would expect to see in average also larger values in other AGN and shock sensitive emission line ratios, such as $[\text{O I}]\lambda 6300/\text{H}\alpha$ or $[\text{S II}]\lambda 6717,6731/\text{H}\alpha$, in barred galaxies when compared to unbarred counterparts. The distributions of the three emission line ratios are shown in Fig. 19. It can clearly be seen that the distributions are only significantly different in the case of $[\text{N II}]\lambda 6583/\text{H}\alpha$, while in the case of $[\text{O I}]\lambda 6300/\text{H}\alpha$ and $[\text{S II}]\lambda 6717,6731/\text{H}\alpha$, the mean values for barred and unbarred galaxies are identical, and the distributions are not statistically different, with AD test P -values greater than 30%, c.f. 0.0009% for $[\text{N II}]\lambda 6583/\text{H}\alpha$.

A difference in nitrogen-to-oxygen abundance ratio in the centres of barred and unbarred galaxies, is then the most

probable explanation for the observed enhancement in the $[\text{N II}]\lambda 6583/\text{H}\alpha$ emission line ratio in barred galaxies. But what can produce an over-abundance of nitrogen with respect to oxygen in barred galaxies?

The N/O abundance ratio is an useful parameter to understand chemical evolution of galaxies (see e.g. Vila Costas & Edmunds 1993; Pérez-Montero & Contini 2009), as both elements are produced by different mechanisms and by stars of different masses. While oxygen is always primary and created in massive stars, nitrogen is synthesized via the CNO and CN cycles in H burning stars and it is mostly secondary (the seed C and O were already present in the placental cloud when the star formed) for metallicity higher than $12+\log(\text{O}/\text{H}) = 8.3$, while for low metallicity very little secondary N is produced. Also, N can be produced in stars of all masses, but mainly in intermediate mass (between 4 and 8 M_{\odot}) stars (Henry et al. 2000). Then, in a single burst of star formation, most of the N is expected to be released to the ISM after O, with a time-delay roughly equal to the stellar lifetime of the main producers of N (intermediate mass stars), i.e. from ~ 100 to 500 Myr after the oxygen was released. Star formation in spiral galaxies might be a continuous process (e.g. Gavazzi & Scodeggio 1996) which complicates the scenario. In addition, gas flows (within the galaxy and from outside) can also in principle alter the initial abundance ratios.

Both chemical evolution models (Mollá & Gavilán 2010) and observational works (Mallery et al. 2007) show that the N/O abundance ratio depends on the star formation history. Simplifying, in a closed-box model, at a fixed metallicity, all that is required for a galaxy or region to increase its N/O is that its current SFR should be less than its past average SFR, so that comparatively fewer high mass stars are being formed now. Then, although newly synthesised oxygen is being released into the ISM from these massive stars currently forming, intermediate-mass stars from the previous generations (when SFR was higher) have had time to evolve and a larger amount of N would be released into the ISM, increasing the N/O abundance ratio. However, metal-poor gas flows have a relatively small effect on the N/O abundance ratio according to models (e.g. Edmunds 1990). While the oxygen abundance is importantly decreased during infall due to dilution of the present gas, the N/O ratio is much less sensitive. The mass infall must be much larger than the galaxy mass (or bulge mass in our case) and the infall rate must be greater than the SFR in order to have large deviations from the expected closed-box behaviour (Köppen & Hensler 2005).

A different history of SF in the centre of barred galaxies with respect to unbarred galaxies is expected from numerical simulations and can at least qualitatively explain the higher N/O abundance ratio observed in bulges less massive than $\sim 10^{9.7} - 10^{10} M_{\odot}$.

Estimating the efficiency of the bar in transporting material to the centre from numerical simulations is not easy because the inflow rate strongly depends on the simulation and the chosen parameters (e.g. Kim et al. 2014). However, it is expected that the efficiency of the bar in driving material to the galaxy centre depends on the bar strength (e.g. Martin & Friedli 1999; Regan & Teuben 2004). The gas flow in the bar potential will form shocks along the bar leading edges, giving way to gas flows towards the centre (e.g. Athanassoula 1992). The availability of gas in the disc will also alter the amount of gas accreted into the bulge region, and as the bar evolves and the gas reservoir diminishes, the inflow rate will also decrease (Athanassoula et al. 2005). Therefore strong gas flows are expected to occur soon after the bar forms, which presumably leads to SF in the inner parts (e.g. Cole et al. 2014). Later on, the bar weakens and gas flows will

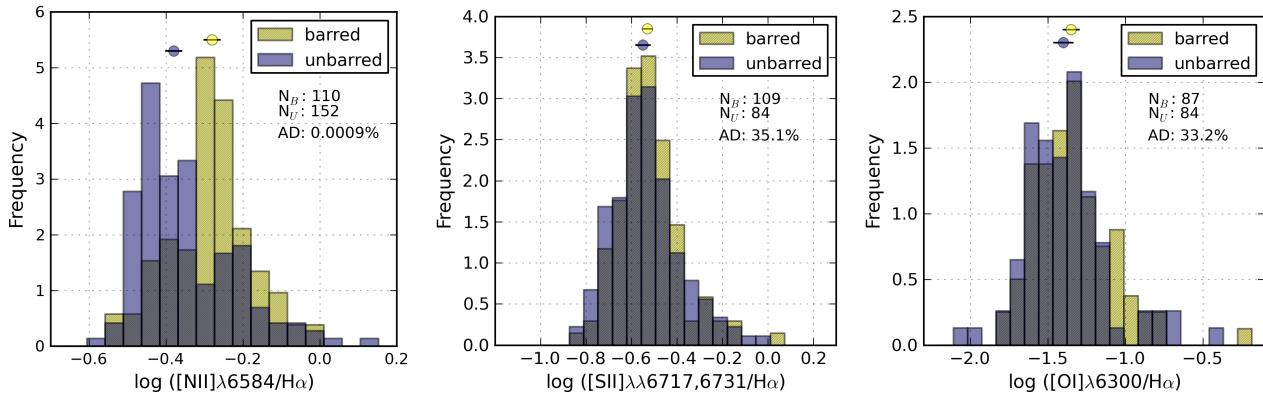


Fig. 19. Histograms showing the distribution of AGN and shock sensitive emission line ratios (from left to right: $[\text{N II}]\lambda 6583/\text{H}\alpha$, $[\text{S II}]\lambda\lambda 6717, 6731/\text{H}\alpha$ and $[\text{O I}]\lambda 6300/\text{H}\alpha$) for barred and unbarred galaxies separately. All galaxies classified as non-AGN are included (see Sec. 4). The barred/unbarred distributions are only different for $[\text{N II}]\lambda 6583/\text{H}\alpha$, and therefore the source of the differences in that line ratio must be other than shock ionisation and/or AGN contamination alone.

still transport material towards the central regions, where it can form stars, but at a lower rate and, according to chemical evolution models, this could explain the high N/O in barred galaxies with respect to unbarred galaxies. Apart from bars, other mechanisms can produce gas flows towards the centre of the galaxies (holding or not a bar), for example tidal forces by an interacting companion (e.g. Cox et al. 2008) or asymmetric structures like spiral arms (e.g. Kormendy & Kennicutt 2004), but these might be more sporadic, not producing a continuous flow as in the case of barred galaxies.

Late-type galaxies have a large reservoir of gas and can therefore supply a large amount of gas towards the centres, given that a considerably strong bar is present. This is not the case for bulge-dominated galaxies, and this might be, at least partially, one of the reasons why differences between barred and unbarred galaxies are smaller or non-existent in galaxies with massive bulges ($\geq 10^{10} M_\odot$). The fact that we do not find differences in central N/O abundance ratio in the most massive bulges could be indicating that bar effects on central gas properties either are negligible (maybe because there is not much gas in the disc to feed the inner parts) or invisible, maybe because there is another and more important and dominant mechanism that masks the expected bar effects.

In any case, for massive bulges (which are also the ones with larger N/O abundance ratio, see Fig. 17) it would be more complicated to detect an increase in N/O in barred galaxies. The reason is that in this scenario of the time-delay in the ejection of N, at high abundances the increase in the N/O abundance ratio is smaller (Coziol et al. 1999). However, the fact that we do not see differences in other properties ($c(\text{H}\beta)$, $12+\log(\text{O}/\text{H})$, $\log U$) or that the differences are smaller (as with Σ_{SFR} or $[\text{S II}]\lambda 6717/[\text{S II}]\lambda 6731$) in the high bulge mass range, points towards a different bulge origin, formation or evolutionary process, dependent on bulge mass (or total galaxy stellar mass).

Bulges are usually classified in two different types: disc-like bulges or pseudo-bulges and classical bulges. The former are generally less massive than classical bulges, and are more common among late-type galaxies. The formation of classical bulges is thought to be faster and normally externally driven, by means of gravitational collapse or hierarchical merging of smaller objects (see e.g. Gadotti 2009 or Athanassoula 2005 for details on the formation mechanisms for the different types), while disc-like bulges are thought to be formed by internal secular pro-

cesses, predominantly driven by bars (e.g. Kormendy & Kennicutt 2004; Athanassoula 2005).

There is observational evidence for a delay in the bar formation for less massive galaxies (Sheth et al. 2012). Therefore, both bars and bulges in massive galaxies, as mentioned before, form at earlier times. These bulges might be classical as they form in more violent environments, with more gas and larger merger rates. Recent numerical simulations (Kraljic et al. 2012) show that the formation of bulges in spiral galaxies is influenced by the bar presence. They find an over abundance of star formation in the bulge for barred galaxies after the bar forms. It is then possible that the difference observed in the central stellar metallicities of massive galaxies Coelho & Gadotti (2011) is set at the time when the bar forms, and consumes and redistributes most of the gas. This would be compatible with the frequent co-existence of both type of bulges in the centres of galaxies as observed in previous works (Peletier et al. 2007; Méndez-Abreu et al. 2014; Erwin et al. 2015). In this scenario, low mass systems will not develop a massive classical bulge, and the bar will form at later times. Furthermore, the central gas accretion will last longer, secularly forming disc-like bulges in barred galaxies. This would generate a difference in the ionised gas properties between barred and unbarred low mass systems as observed in the present work.

Therefore our result that central properties of ionised gas differ predominantly in galaxies with lower mass bulges, gives strength to a different origin or evolutionary process for less and more massive bulges, with the gaseous phase of the former having currently a closer relation with bars.

12.2. Comparison with recent works

Several works have tried to find observational evidence for the effect of gas flows by analysing the gas content, SFRs and/or metallicities in galaxy centres (e.g. Ho et al. 1997b; Martin & Friedli 1999) but results were inconclusive, in part because these works were carried out with small data samples and sample selections could have introduced biased results due to well known now relations between the analysed gas properties with Hubble type and/or total stellar mass. In an effort to circumvent these problems, more recently Ellison et al. (2011) and Cacho et al. (2014) have comparatively analysed gaseous-phase metallicities and SFRs in the centres of barred and unbarred galaxies in large samples (from ~ 900 to 1500 galaxies respectively) by us-

ing SDSS spectra. In both cases the galaxy samples have been taken from the catalogue of Nair & Abraham (2010)¹², requiring axial ratios $b/a \geq 0.4$ (i.e. $i \leq 68^\circ$, c.f. to 26° in our sample) and redshift range $z \leq 0.06$ and $z < 0.1$ in Ellison et al. (2011) and Cacho et al. (2014), respectively. Special care was taken by these authors to avoid biases due to differences in inclination, redshift and stellar mass between their barred and unbarred galaxy samples. However, and in spite of the similarity in their samples and in the data analysis, they find different results. While Ellison et al. (2011) find that the SFR and the oxygen abundance in the galaxy centres are considerably larger in barred galaxies more massive than $10^{10} M_\odot$ with respect to unbarred galaxies of the same mass, Cacho et al. (2014) do not find statistically significant differences between barred and unbarred galaxies, but a trend (which decreases with increasing mass) in their early-type subsample, for barred galaxies to exhibit a larger $12+\log(O/H)$ than unbarred galaxies.

The study presented here is in apparent disagreement with both Ellison et al. (2011) and Cacho et al. (2014), as we do find significant differences between barred and unbarred galaxies, but we do not see differences in the oxygen abundance between barred and unbarred galaxies. However, our results can explain in a large extent the disagreement of Ellison et al. (2011) and Cacho et al. (2014) results among themselves and with ours. It mostly comes from the way in which star-forming galaxies are selected and the empirical calibration used to obtain oxygen abundances. Cacho et al. (2014) use Kauffmann et al. (2003a) to separate star-forming dominated from active galaxies, which rejects galaxies from the *transition area*, where pure star-forming galaxies with high nitrogen abundance are expected to be located (e.g. Pérez-Montero & Contini 2009). Ellison et al. (2011) and ourselves use Kewley et al. (2001) and therefore include *transition* objects in our analysis and our samples are then expected to contain more nitrogen-rich galaxy centres. In addition, Ellison et al. (2011) use the $[N II]/[O II]$ empirical calibration (Kewley & Dopita 2002) to obtain $12+\log(O/H)$, which depends on the N/O abundance. We believe their reported larger $12+\log(O/H)$ in barred galaxies might be indicating a larger N/O abundance ratio in barred with respect to unbarred galaxies. Cacho et al. (2014) use the R_{23} parameter to obtain oxygen abundances, but later on, in an effort to explain the differences with Ellison's results, they apply the same empirical calibration as Ellison et al. (2011), $[N II]/[O II]$. With this calibration they also find larger $12+\log(O/H)$ in barred than in unbarred galaxies, but the difference is not as significant as in Ellison et al. (2011) because their sample lacks a significant number of nitrogen rich galaxies as explained above. We also get larger $12+\log(O/H)$ in barred galaxies when using empirical calibrations involving $[N II]\lambda 6584$ such as the ones given by Pettini & Pagel (2004); Kewley & Dopita (2002) or Bresolin (2007), but no difference when R_{23} or the Pérez-Montero (2014) method is used, as described in Sec. 6.

Finally, we would like to mention that the fact that Ellison et al. (2011) only find differences in the most massive galaxies of their sample ($M_\star \gtrsim 10^{10} M_\odot$) does not contradict our results, as our galaxy sample contains galaxies precisely more massive than $10^{10} M_\odot$. Our results do differ in that we do not find differences between barred and unbarred galaxies more massive than $\sim 10^{10.8} M_\odot$, while Ellison et al. (2011) finds larger SFRs and $12+\log(O/H)$ up to their upper limit mass ($\sim 10^{11.2} M_\odot$).

We believe that the results presented here are showing the footprints of bar-induced secular evolution of galaxies in the central gaseous component, which seems to be either more ef-

ficient or more relevant in galaxies with less massive bulges (i.e. later type galaxies), at least regarding the current central properties of the gas.

13. Summary and conclusions

We have analysed the properties of the ionised gas in the centre of a sample containing 251 and 324 barred and unbarred face-on galaxies respectively (173 and 265 after removing AGN, Kewley et al. 2001) of total stellar masses between 10^{10} and $10^{11.2} M_\odot$, where both subsamples have the same total galaxy stellar mass and redshift distributions. We have compared the distributions of internal extinction at $H\beta$, SFR per unit area (Σ_{SFR}), $[S II]\lambda\lambda 6717, 6731$ emission line ratio, empirical tracers of oxygen abundance (R_{23} and $N2=[N II]\lambda 6854/H\alpha$), oxygen abundance, nitrogen-to-oxygen abundance ratio and ionisation parameters, for barred and unbarred galaxies separately. Our main conclusions are:

- The whole non-AGN barred galaxy sample has statistically significant different distributions of $c(H\beta)$, Σ_{SFR} , $[S II]\lambda\lambda 6717, 6731$, $N2$ and $\log(N/O)$ in their centres with respect to unbarred galaxies. The differences are remarkably evident in $N2$ and $\log(N/O)$, which are ~ 0.1 dex larger in barred than in unbarred galaxies. Barred galaxies also tend to have larger central internal extinction, Σ_{SFR} , and electron density than unbarred galaxies, but in these cases the differences in median values between both distributions are within errors. We do not find differences between barred and unbarred galaxies neither in the central value of the R_{23} parameter, nor in $12+\log(O/H)$ as determined from Pérez-Montero (2014) grids of photoionisation models.
- When we split our sample into earlier and later types (according to their B/D light ratio or their bulge mass), the differences enhance towards later type galaxies. Specially significant is the difference in $N2$, which is ~ 0.13 dex larger in late-type barred with respect to unbarred galaxies, against a difference of ~ 0.07 dex between barred and unbarred galaxies in the earlier-type subsample. This difference in $N2$ translates in a difference in N/O abundance ratio of 0.09 - 0.12 dex from photoionisation models. With this separation into earlier and later types, the oxygen abundance distribution appears to be different in barred and unbarred late-type galaxies, with a slightly larger median value for unbarred galaxies. There is no difference in $12+\log(O/H)$ between barred and unbarred galaxies in the early-type subsample. In addition to $12+\log(O/H)$, barred and unbarred early-type galaxies seem to have similar central $c(H\beta)$, R_{23} and $\log U$. The distributions of Σ_{SFR} and N/O are different in barred and unbarred early-type galaxies (towards larger values in barred galaxies) depending on the way we separate early from late type galaxies.
- We have explored the above barred/unbarred parameter differences in terms of the galaxy total and bulge stellar mass. These increase towards galaxies with lower mass systems and seem to correlate better with bulge mass except for the SFR per unit area, which seems to have a stronger dependence with total galaxy stellar mass.
- We find no clear relation between the central ionised gas properties in barred galaxies and the bar structural parameters (effective radius, bar length, ellipticity or bar Sersic index), but weak trends for the central Σ_{SFR} to increase with bar effective length.

¹² Bars are visually classified in the Nair & Abraham (2010) catalogue.

- The differences observed between barred and unbarred galaxies can qualitatively be explained with current knowledge on bar evolution simulations and chemical evolution models.

Taking all together, our results imply that bars do alter the properties of the central ionised gas of galaxies, increasing their electron density, internal extinction, SFR per unit area, and very notably the N/O abundance ratio. These bar effects on central ionised gas are more visible in later type galaxies, or more precisely, in those with bulges less massive than $\sim 10^{10} M_{\odot}$.

This work presents one of the clearest observational evidences so far for the effects of bars in galaxy centres. It also emphasizes (1) the usefulness of the nitrogen-to-oxygen abundance ratio, which gives important clues on the star formation history of galaxy centres, and (2) the risk of using certain empirical calibrations for oxygen abundance estimations, which can mask a high N/O under a fake high O abundance.

Acknowledgements. We acknowledge Joerg Dietrich for kindly sharing with us his python script to perform the k -sample Anderson-Darling test and William Schoenell for help in understanding STARLIGHT output spectra. This work has been supported by MICINN of Spain via grants AYA2011-24728 (EF, IP and AZ), FPA2010-16802 (EF) and AYA2010-21887-C04-01 (EPM), and from the “Junta de Andalucía” local government through the FQM-108 project (AZ, IP and EF).

References

- Anderson, T. W. & Darling, D. A. 1954, *Journal of the American Statistical Association*, 49, 765
- Athanassoulas, E. 1992, *MNRAS*, 259, 345
- Athanassoulas, E. 2003, *MNRAS*, 341, 1179
- Athanassoulas, E. 2005, *MNRAS*, 358, 1477
- Athanassoulas, E., Lambert, J. C., & Dehnen, W. 2005, *MNRAS*, 363, 496
- Athanassoulas, E., Machado, R. E. G., & Rodionov, S. A. 2013, *MNRAS*, 429, 1949
- Baldwin, J. A., Phillips, M. M., & Terlevich, R. 1981, *PASP*, 93, 5
- Barnes, J. E. & Hernquist, L. 1992, *ARA&A*, 30, 705
- Bothwell, M. S., Maiolino, R., Kennicutt, R., et al. 2013, *MNRAS*, 433, 1425
- Bournaud, F. & Combes, F. 2002, *A&A*, 392, 83
- Bresolin, F. 2007, *ApJ*, 656, 186
- Bresolin, F. & Kennicutt, Jr., R. C. 2002, *ApJ*, 572, 838
- Cacho, R., Sánchez-Blázquez, P., Gorgas, J., & Pérez, I. 2014, *MNRAS*, 442, 2496
- Calzetti, D., Armus, L., Bohlin, R. C., et al. 2000, *ApJ*, 533, 682
- Cardelli, J. A., Clayton, G. C., & Mathis, J. S. 1989, *ApJ*, 345, 245
- Chapelon, S., Contini, T., & Davoust, E. 1999, *A&A*, 345, 81
- Cheung, E., Athanassoulas, E., Masters, K. L., et al. 2013, *ApJ*, 779, 162
- Cid Fernandes, R., Mateus, A., Sodré, L., Stasińska, G., & Gomes, J. M. 2005, *MNRAS*, 358, 363
- Coelho, P. & Gadotti, D. A. 2011, *ApJ*, 743, L13
- Cole, D. R., Debattista, V. P., Erwin, P., Earp, S. W. F., & R., R. 2014, *astro-ph*, 100
- Considère, S., Coziol, R., Contini, T., & Davoust, E. 2000, *A&A*, 356, 89
- Coziol, R., Reyes, R. E. C., Considère, S., Davoust, E., & Contini, T. 1999, *A&A*, 345, 733
- de Souza, R. E., Gadotti, D. A., & dos Anjos, S. 2004, *ApJS*, 153, 411
- Denicoló, G., Terlevich, R., & Terlevich, E. 2002, *MNRAS*, 330, 69
- Díaz, Á. I., Terlevich, E., Castellanos, M., & Hägele, G. F. 2007, *MNRAS*, 382, 251
- Dors, Jr., O. L., Krabbe, A., Hägele, G. F., & Pérez-Montero, E. 2011, *MNRAS*, 415, 3616
- Dors, Jr., O. L., Storch-Bergmann, T., Riffel, R. A., & Schimdt, A. A. 2008, *A&A*, 482, 59
- Dutil, Y. & Roy, J.-R. 1999, *ApJ*, 516, 62
- Edmunds, M. G. 1990, *MNRAS*, 246, 678
- Edmunds, M. G. & Pagel, B. E. J. 1978, *MNRAS*, 185, 77P
- Ellison, S. L., Nair, P., Patton, D. R., et al. 2011, *MNRAS*, 416, 2182
- Erwin, P. 2005, *MNRAS*, 364, 283
- Erwin, P., Saglia, R. P., Fabricius, M., et al. 2015, *MNRAS*, 446, 4039
- Florido, E., Pérez, I., Zurita, A., & Sánchez-Blázquez, P. 2012, *A&A*, 543, A150
- Friedli, D. & Benz, W. 1993, *A&A*, 268, 65
- Friedli, D., Benz, W., & Kennicutt, R. 1994, *ApJ*, 430, L105
- Gadotti, D. A. 2008, *MNRAS*, 384, 420
- Gadotti, D. A. 2009, *MNRAS*, 393, 1531
- Gavazzi, G. & Scodreggio, M. 1996, *A&A*, 312, L29
- Graham, A. W. & Worley, C. C. 2008, *MNRAS*, 388, 1708
- Henry, R. B. C., Edmunds, M. G., & Köppen, J. 2000, *ApJ*, 541, 660
- Ho, L. C., Filippenko, A. V., & Sargent, W. L. W. 1997a, *ApJ*, 487, 579
- Ho, L. C., Filippenko, A. V., & Sargent, W. L. W. 1997b, *ApJ*, 487, 591
- Hou, A., Parker, L. C., Harris, W. E., & Wilman, D. J. 2009, *ApJ*, 702, 1199
- Howarth, I. D. 1983, *MNRAS*, 203, 301
- Hummel, E., van der Hulst, J. M., Kennicutt, R. C., & Keel, W. C. 1990, *A&A*, 236, 333
- Kauffmann, G., Heckman, T. M., Tremonti, C., et al. 2003a, *MNRAS*, 346, 1055
- Kauffmann, G., Heckman, T. M., White, S. D. M., et al. 2003b, *MNRAS*, 341, 33
- Kennicutt, Jr., R. C. 1998, *ApJ*, 498, 541
- Kennicutt, Jr., R. C., Keel, W. C., & Blaha, C. A. 1989, *AJ*, 97, 1022
- Kewley, L. J. & Dopita, M. A. 2002, *ApJS*, 142, 35
- Kewley, L. J., Dopita, M. A., Sutherland, R. S., Heisler, C. A., & Trevena, J. 2001, *ApJ*, 556, 121
- Kewley, L. J., Groves, B., Kauffmann, G., & Heckman, T. 2006, *MNRAS*, 372, 961
- Kim, T., Sheth, K., Gadotti, D. A., et al. 2014, *ArXiv e-prints*
- Kobulnicky, H. A. & Kewley, L. J. 2004, *ApJ*, 617, 240
- Köppen, J. & Hensler, G. 2005, *A&A*, 434, 531
- Kormendy, J. & Kennicutt, Jr., R. C. 2004, *ARA&A*, 42, 603
- Kraljic, K., Bournaud, F., & Martig, M. 2012, *ApJ*, 757, 60
- Kreckel, K., Groves, B., Schinnerer, E., et al. 2013, *ApJ*, 771, 62
- López-Hernández, J., Terlevich, E., Terlevich, R., et al. 2013, *MNRAS*, 430, 472
- López-Sánchez, Á. R., Dopita, M. A., Kewley, L. J., et al. 2012, *MNRAS*, 426, 2630
- Mallery, R. P., Kewley, L., Rich, R. M., et al. 2007, *ApJS*, 173, 482
- Martel, H., Kawata, D., & Ellison, S. L. 2013, *MNRAS*, 431, 2560
- Martin, P. & Friedli, D. 1999, *A&A*, 346, 769
- Martinet, L. & Friedli, D. 1997, *A&A*, 323, 363
- McGaugh, S. S. 1991, *ApJ*, 380, 140
- Meisels, A. & Ostriker, J. P. 1984, *AJ*, 89, 1451
- Méndez-Abreu, J., Debattista, V. P., Corsini, E. M., & Aguerri, J. A. L. 2014, *A&A*, 572, A25
- Mollá, M. & Gavilán, M. 2010, *Mem. Soc. Astron. Italiana*, 81, 992
- Nagao, T., Maiolino, R., & Marconi, A. 2006, *A&A*, 459, 85
- Nair, P. B. & Abraham, R. G. 2010, *ApJS*, 186, 427
- O'Donnell, J. E. 1994, *ApJ*, 422, 158
- Oh, K., Sarzi, M., Schawinski, K., & Yi, S. K. 2011, *ApJS*, 195, 13
- Oh, S., Oh, K., & Yi, S. K. 2012, *ApJS*, 198, 4
- Osterbrock, D. E. & Ferland, G. J. 2006, *Astrophysics of gaseous nebulae and active galactic nuclei*
- Pagel, B. E. J., Edmunds, M. G., Blackwell, D. E., Chun, M. S., & Smith, G. 1979, *MNRAS*, 189, 95
- Peletier, R. F., Falcón-Barroso, J., Bacon, R., et al. 2007, *MNRAS*, 379, 445
- Pérez-Montero, E. 2014, *MNRAS*, 441, 2663
- Pérez-Montero, E. & Contini, T. 2009, *MNRAS*, 398, 949
- Pérez-Montero, E. & Díaz, A. I. 2005, *MNRAS*, 361, 1063
- Pettini, M. & Pagel, B. E. J. 2004, *MNRAS*, 348, L59
- Pfenniger, D. & Norman, C. 1990, *ApJ*, 363, 391
- Pilyugin, L. S. 2001, *A&A*, 369, 594
- Pilyugin, L. S. & Thuan, T. X. 2005, *ApJ*, 631, 231
- Pompea, S. M. & Rieke, G. H. 1990, *ApJ*, 356, 416
- Regan, M. W. & Teuben, P. J. 2004, *ApJ*, 600, 595
- Regan, M. W., Vogel, S. N., & Teuben, P. J. 1997, *ApJ*, 482, L143
- Roussel, H., Sauvage, M., Vigroux, L., et al. 2001, *A&A*, 372, 406
- Sakamoto, K., Okumura, S. K., Ishizuki, S., & Scoville, N. Z. 1999, *ApJ*, 525, 691
- Sanchez, S. F., Perez, E., Rosales-Ortega, F. F., et al. 2014, *ArXiv e-prints*
- Schlegel, D. J., Finkbeiner, D. P., & Davis, M. 1998, *ApJ*, 500, 525
- Scholz, F. W. & Stephens, M. A. 1987, *Journal of the American Statistical Association*, 82, 918–924
- Seaton, M. J. 1979, *MNRAS*, 187, 73P
- Sellwood, J. A. & Wilkinson, A. 1993, *Reports on Progress in Physics*, 56, 173
- Shaw, R. A. & Dufour, R. J. 1994, in *Astronomical Society of the Pacific Conference Series*, Vol. 61, *Astronomical Data Analysis Software and Systems III*, ed. D. R. Crabtree, R. J. Hanisch, & J. Barnes, 327
- Shen, J. & Sellwood, J. A. 2004, *ApJ*, 604, 614
- Sheth, K., Melbourne, J., Elmegreen, D. M., et al. 2012, *ApJ*, 758, 136
- Sheth, K., Vogel, S. N., Regan, M. W., Thornley, M. D., & Teuben, P. J. 2005, *ApJ*, 632, 217
- Shlosman, I., Frank, J., & Begelman, M. C. 1989, *Nature*, 338, 45
- Stasińska, G., Mateus, Jr., A., Sodré, Jr., L., & Szczerba, R. 2004, *A&A*, 420, 475
- Stauffer, J. R. 1982, *ApJ*, 262, 66
- Stephens, M. A. 1974, *Journal of the American Statistical Association*, 347, 730
- Storch-Bergmann, T., Calzetti, D., & Kinney, A. L. 1994, *ApJ*, 429, 572
- Tremonti, C. A., Heckman, T. M., Kauffmann, G., et al. 2004, *ApJ*, 613, 898
- Vazdekis, A., Sánchez-Blázquez, P., Falcón-Barroso, J., et al. 2010, *MNRAS*, 404, 1639
- Vila Costas, M. B. & Edmunds, M. G. 1993, *MNRAS*, 265, 199
- Wang, J., Kauffmann, G., Overzier, R., et al. 2012, *MNRAS*, 423, 3486
- Willett, K. W., Lintott, C. J., Bamford, S. P., et al. 2013, *MNRAS*, 435, 2835
- Zhou, Z.-M., Cao, C., & Wu, H. 2015, *AJ*, 149, 1
- Zurita, A., Relaño, M., Beckman, J. E., & Knapen, J. H. 2004, *A&A*, 413, 73

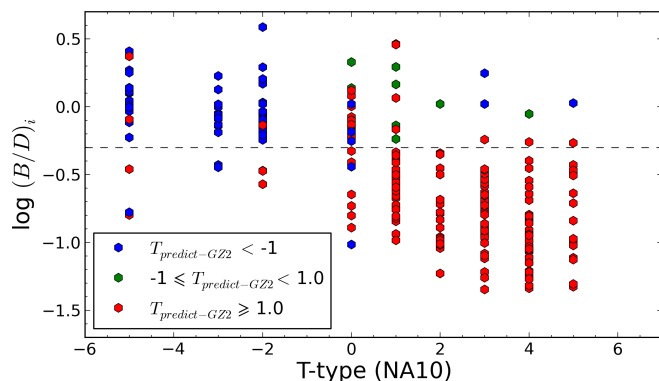


Fig. A.2. Decimal logarithm of the bulge-to-disc flux ratio in the i -band as a function of the morphological T-type as given in the Nair & Abraham (2010) catalogue for the galaxies of our sample included in this catalogue. The colours represent different values of the predicted T-type Galaxy Zoo 2 parameter Willett et al. (2013).

Appendix A: Bulge-to-Disc flux ratios for different galaxy morphological types.

The decrease of the B/D flux ratio along the Hubble sequence from early to later-type galaxies is well known, but among others, it depends on the galaxy structural component fitting procedure, on inclination and dust-extinction (see Graham & Worley 2008, and references therein). Morphological classification is only available, from the largest catalogue so far Nair & Abraham (2010), for less than 50% of our galaxy sample. Our aim here is to use the B/D flux ratios (Gadotti 2009) and the morphological classification in T-types for our subsample of galaxies included in the Nair & Abraham (2010) catalogue, to separate our galaxies into early and late-types, according to their B/D flux ratios.

Fig. A.1 shows the dependence of the logarithm of the g , r and i -band B/D light ratios obtained with BUDDA (Gadotti 2009) with the T-type by Nair & Abraham (2010) for the barred and unbarred galaxies in common between both samples. The top and bottom-left panels show this relation for the three different photometric bands, with small crosses for unbarred galaxies and small filled circles for barred galaxies. The large crosses and big empty circles indicate the median $\log(B/D)$ value for each T-type value for unbarred and barred galaxies respectively. As it can be seen there are no clear differences for barred and unbarred galaxies. The bottom-right panel shows the median $\log(B/D)$ values, for barred and unbarred galaxies together, for each T-type for all photometric bands. The differences in the median B/D light ratio between the different bands are in general smaller than the error bars.

Our median values agree well (within error bars) with those from Graham & Worley (2008, their Fig. 6) in the T-type range in common (between T-type 0 and 5), except for T=0 in which we obtain a marginally larger B/D ratio in the r and i bands. These differences could arise from poor statistics at T=0 in Graham & Worley (2008) (only 3 galaxies versus 30 in our subsample of galaxies included in the Nair & Abraham (2010) catalogue).

We caution the reader that a number of unbarred galaxies in our sample (~ 15), supposed to be disc galaxies, are classified with T-type ≤ -3 by Nair & Abraham (2010), i.e. as ellipticals (see Fig. A.1 or A.2). These galaxies are very difficult to classify, since a face-on disc without spiral arms or a bar looks just like a round elliptical. Gadotti (2009) classified as disc galaxies after looking at isophotal contours and the profile very carefully,

but as stated in the cited paper, the estimated misclassification frequency is ~ 5 -10%. With these uncertainties in mind, we have opted to keep them in our galaxy sample and consider them as S0 disc galaxies.

The bulge-to-disc flux ratios decrease towards late-type spirals as expected. We have used this trend to create subsamples dominated by early or late-type spirals. In our subsample of galaxies included in the Nair & Abraham (2010) catalogue, a value of $\log(B/D) = -0.30$ (or $B/D = 0.5$) approximately separates galaxies with T-type < 2 (earlier than Sa) from those later or equal to T-type $= 2$ (Sab), but the contamination from late-types (with the previous definition) in the early-type subsample and vice versa is of order 12% and 30% respectively. The predicted T-type, as given in the Galaxy Zoo2¹³ catalogue (hereinafter GZ2 Willett et al. 2013), permits to improve this separation. We then consider early-type galaxies as those galaxies of the sample with $B/D \geq 0.5$ or those that having $B/D < 0.5$ have a T-type, as predicted by GZ2, lower than -1. Similarly, we consider as late-type galaxies those with $B/D < 0.5$ and a T-type as predicted by GZ2, larger or equal than 1. In this way we are able to include $\sim 70\%$ and 90% of the early (T-type < 2) and late types (T-type ≥ 2) in the subsamples of early and late-type galaxies respectively, and the contamination from late (early-types) in the early (late-type) subsample is $\sim 10\%$ (25%). These numbers are the same in all three bands. However, we have used the i -band, as the B/D flux ratio is available for all sample galaxies in this filter.

¹³ <http://data.galaxyzoo.org/>

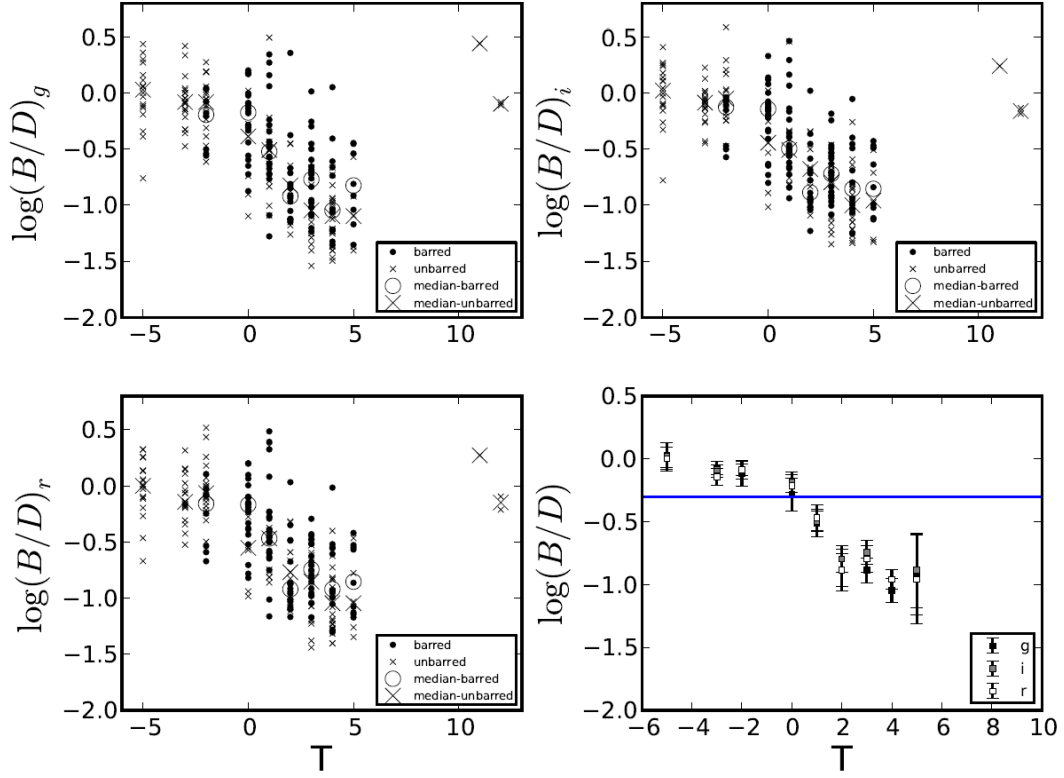


Fig. A.1. Logarithm of the bulge-to-disc (B/D) flux ratio in the g , r and i -band versus morphological type (expressed as T -type) for the galaxies of the sample contained in the Nair & Abraham (2010) catalogue. Big crosses and big empty circles mark the median $\log(B/D)$ for each T -type value for unbarred and barred galaxies respectively. The bottom-right panel shows the median $\log(B/D)$ in each band for each T -type value. Error bars represent the 95% confidence level of the median value for the distribution of B/D values at each T -type value. The blue solid straight line marks $B/D = 0.5$, that we have used to separate early from late-type galaxies.